MATERIALS CHEMISTRY
FRONTIERS

REVIEW

View Article Online
View Journal | View Issue

Cite this: *Mater. Chem. Front.*, 2024, **8**, 2109

Optimization strategies for key interfaces of LLZO-based solid-state lithium metal batteries

Jiangwei Chu,†[ab] Ziwei Li,†[ac] Jin Wang,†[a] Gang Huang*[ab] and Xinbo Zhang *[ab]

Solid-state lithium metal batteries (SSLMBs) are believed to be next-generation energy storage systems owing to their superior safety performance and higher energy density compared with state-of-the-art lithium-ion batteries. Solid-state electrolytes (SSEs), as the most critical component of solid-state batteries (SSBs), determine the performance of the batteries to a large extent. Among different types of SSEs, the garnet-type $Li_7La_3Zr_2O_{12}$ (LLZO) has an exceptionally high ionic conductivity (10^{-3} to 10^{-4} S cm^{-1}) and good chemical stability against lithium metal, providing a fantastic possibility for use in SSLMBs. However, developing usable, accessible LLZO-based SSLMBs is still a difficult task owing to the interfacial issues. This review concentrates on the key interfaces of LLZO-based SSLMBs, including lithium metal/LLZO interfaces, LLZO/cathode interfaces, and internal interfaces of LLZO-based SSEs. The main challenges and corresponding strategies for interface optimization are thoroughly covered. Comprehensive research models and advanced characterization tools deployed and developed to study the aforementioned issues are also outlined. Additionally, effective solutions from the perspective of engineering applications are highlighted. Finally, perspectives for future research are provided to guide the development of LLZO-based SSLMBs.

Received 13th October 2023,
Accepted 8th January 2024

DOI: 10.1039/d3qm01111a

rsc.li/frontiers-materials

1. Introduction

Secondary batteries with high energy density and exceptional safety are desperately needed with the surge in electric vehicles and grid energy storage. Currently, lithium-ion batteries are widely used in the electric-vehical field as a source of power. Lithium-ion batteries assembled with silicon–carbon anodes and high-nickel transition-metal-oxide cathodes have achieved a high energy density of 360 W h kg^{-1}, which is practically at their maximum.[1,2] However, this is far from sufficient to match people's expectations for long-lasting electric equipment. Furthermore, liquid organic electrolytes usually used in lithium-ion batteries have the potential to burn and explode. To overcome the above-mentioned challenges, a new battery system must be developed.

Lithium metal is regarded as the best anode because it possesses the largest theoretical specific capacity of 3680 mA h g^{-1} and

[a] *State Key Laboratory of Rare Earth Resource Utilization, Changchun Institute of Applied Chemistry, Chinese Academy of Sciences, Changchun 130022, P. R. China. E-mail: ghuang@ciac.ac.cn, xbzhang@ciac.ac.cn*
[b] *School of Applied Chemistry and Engineering, University of Science and Technology of China, Hefei 230026, P. R. China*
[c] *Key Laboratory of Automobile Materials, Ministry of Education and Department of Materials Science and Engineering, Jilin University, Changchun 130022, China*
† These authors contributed equally to this work.

Jiangwei Chu

Jiangwei Chu obtained his BE from Northeastern University (NEU) in 2020. He is currently pursuing his PhD in the Academy of Applied Chemistry and Engineering at the University of Science and Technology of China. His research focuses on solid-state electrolytes for Li-metal batteries.

Ziwei Li

Ziwei Li received his BE from Jilin University (JLU) in 2018. He is currently a PhD candidate at JLU and is being mentored at the Changchun Institute of Applied Chemistry (CIAC). His current research interests include the interface design of Li-metal batteries.

the lowest electrode potential of −3.04 V *versus* the standard hydrogen electrode.[3–5] Lithium metal batteries with transition metal oxide cathodes are capable of delivering a high energy density up to 440 W h kg^{-1}.[6,7] However, lithium metal batteries would raise new security issues such as lithium dendrites piercing membranes and consequently causing short circuits.[8,9] Solid-state electrolytes (SSEs), which differ from the liquid organic electrolytes in their density, high modulus and thermal stability, can both avoid the safety risks associated with the liquid organic electrolytes and inhibit the growth of lithium dendrites.[10–14] Therefore, solid-state lithium metal batteries (SSLMBs) assembled with lithium metal and SSEs have attracted widespread attention.

Inorganic SSEs and polymer SSEs are the two main categories of SSEs. The principal inorganic SSEs are garnet electrolytes, NASICON electrolytes, sulfide electrolytes, oxynitride electrolytes, and halide electrolytes. Among these, $Li_7La_3Zr_2O_{12}$ (LLZO), the most typical garnet-type SSE, offers the greatest significant promise for SSLMBs due to its high ionic conductivity, wide electrochemical window, and good stability against Li metal.[15–19] Since Weppner's group discovered the cubic-phase LLZO, the ionic conductivity of LLZO has been continuously increased to above 1 mS cm^{-1}, which is comparable to the ionic conductivity of the conventional liquid electrolyte.[20,21] In the past ten years, a significant amount of experimental data and simulation findings have revealed that interface issues, including poor interface stability, slow ion transport, and high interface impedance, substantially limit the performance of LLZO-based SSLMBs.[22–25] Undoubtedly, understanding and solving the interface problems are indispensable for achieving high-performance, high-safety LLZO-based SSLMBs.

In this review, we concentrate on reviewing the progresses in the key interfaces of LLZO-based SSLMBs including lithium metal/LLZO interfaces, LLZO/cathode interfaces, as well as internal interfaces of LLZO-based SSEs. First, a summary of the origin of interface problems and corresponding strategies is given. Second, advanced characterization techniques and comprehensive research models for studying the aforementioned issues are highlighted. Third, the interface problem solutions from the viewpoint of engineering are discussed. In the end, we provide perspectives for the development of LLZO-based SSLMBs.

2. Lithium metal/LLZO interfaces

LLZO is stable against lithium metal, which is one of the factors driving research into LLZO-based SSLMBs. However, there are still substantial problems with lithium dendrites and high interface impedance at the lithium metal/LLZO interface. High interface impedance would lead to severe polarization and reduce the energy conversion efficiency. Severe lithium dendrites cause short circuits, premature death of battery, and even serious safety issues. Obviously, reducing interface impedance and suppressing lithium dendrites are key issues for developing LLZO-based SSLMBs. For this, the reasons for high interface impedance and lithium dendrites will be discussed in the below section, followed by discussions of the relevant methods.[22,26,27]

2.1 Causes of large interface impedance

The lithium metal/LLZO interface actually shows point-to-point contacts, mostly due to a lithiophobic Li_2CO_3 layer that grows on the LLZO surface.[28–31] The contact angle between LLZO with Li_2CO_3 and molten lithium metal exceeds 90°, showing the non-wetting of LLZO by lithium metal.[32] In addition, the lithium metal anode also undergoes significant volume change

Jin Wang

Jin Wang received her PhD from Jilin University in 2021. Now she is an assistant professor at the Changchun Institute of Applied Chemistry (CIAC). Her current interests include the design and synthesis of solid-state electrolytes for Li-metal batteries and Li metal protection.

Gang Huang

Gang Huang received his PhD in applied chemistry from the Changchun Institute of Applied Chemistry (CIAC) in 2016. Now he is a full professor at CIAC. His research focuses on the design of composite electrolytes and dendrite-free metal anodes for high-energy metal-based batteries.

Xinbo Zhang

Xinbo Zhang is a full professor at the Changchun Institute of Applied Chemistry (CIAC), Chinese Academy of Sciences (CAS). He obtained his PhD degree in inorganic chemistry from CIAC in 2005. His interests mainly focus on functional inorganic materials for batteries, fuel cells, and electrochemical catalysis.

during dissolution and deposition processes, which results in interface degradation and rising impedance.[33,34] Removing Li_2CO_3 and delaying the interface degradation are significant solutions to reduce high interface impedance.

2.2 Causes of lithium dendrite formation

LLZO has a shear modulus as high as 56–61 GPa, which is obviously higher than the required value for preventing dendrite initiate (8.5 GPa).[35] However, lithium dendrites still grow and even penetrate LLZO during battery cycling.[36,37] Two widely accepted theories have emerged from in-depth studies on the genesis of lithium dendrites. The first view attributes lithium dendrites to the interfacial non-uniformity associated with micro-structural defect and poor contact of the lithium metal/LLZO interface, which may lead to high local current density and then cause nonuniform lithium deposition.[38,39] Another theory is that lithium metal deposits directly inside LLZO due to LLZO's non-negligible electrical conductivity. More crucially, there is a significant enhancement in electronic conductivity close to grain boundaries or flaws. Furthermore, according to theoretical and experimental findings, the elastic modulus at grain boundaries is roughly 50% lower than that at grains, which facilitates the growth of lithium dendrites along grain boundaries.[40,41] Therefore, these defects could serve as electron conduction channels that allow lithium metal to nucleate and grow more easily.[42–45]

2.3. Strategies for reducing interface impedance and inhibiting lithium dendrites

Among the various strategies, removing Li_2CO_3 and adding interlayers are the most effective and popular. The methods for eliminating Li_2CO_3 include physical polishing, high-temperature calcination, and conversion reaction. The interlayers can be divided into three categories: electron conductive layers, ion conductive layers, and mixed ion/electron conductive layers (MCL).

2.3.1 Removal of Li_2CO_3. Both physical procedures and chemical approaches can be used to remove Li_2CO_3. A popular physical technique for eliminating Li_2CO_3 is mechanical polishing. After sanding and polishing with sandpapers, Li_2CO_3 on the surface of the Ta-doped LLZO (LLZTO) sheet is removed, and the molten lithium metal can be spread on polished LLZTO.[46] To get rid of surface impurities on LLZTO, Mao *et al.* adopted an ultra-high-speed mechanical polishing technique. The complete elimination of Li_2CO_3 was facilitated by the strong centrifugal force produced by high-speed rotation, which restored the lithiophilic properties of LLZTO. The contact impedance was decreased to 28.15 O cm^2 due to the extremely clean surface (Fig. 1a).[47] Although physical polishing is efficient, it cannot completely remove all of the Li_2CO_3 contaminants inside LLZO. Many researchers choose chemical methods such as high-temperature decomposition and conversion reaction to remove Li_2CO_3. Guo and colleagues effectively cleaned Li_2CO_3 inside LLZO by calcination at a high temperature of 900 1C. Li_2CO_3-free LLZO demonstrated lithiophilic characteristics without surface modification, raising the critical current densities (CCD).[28] Grey *et al.* heated air-exposed LLZO under oxygen at 500 1C, achieving complete regeneration of LLZO and low lithium metal/LLZO interfacial resistance (10 O cm^2).[48] Although Li_2CO_3 can be removed by high-temperature calcination, more lithium volatilization happens concurrently, and additional contaminants are also produced. In addition, high-temperature calcination is generally energy-consuming and time-consuming. It is worth to explore low-temperature treatment to remove Li_2CO_3.

Utilizing the conversion reaction between Li_2CO_3 and some substances can easily get rid of Li_2CO_3 at low temperatures. Since inorganic acids such as HCl, H_3PO_4, and HF may completely and swiftly react with Li_2CO_3 at ambient temperature, acid treatment has a potential effect on eliminating Li_2CO_3.[32,49–51] Zhai *et al.* dropped 40% HF solution to the surface of LLZTO, not only Li_2CO_3 was removed, but also the LiF/LaF_3-rich 3D-burr-microsphere (BM) interface layer was generated on the surface of LLZTO. The 3D-BM interface layer with a large specific surface area showed super-lithiophilicity, enabling the facile infiltration of molten lithium metal (Fig. 1b). The assembled symmetrical cells achieved a high CCD of 2.7 mA cm^{-2} at room temperature and an ultra-low interface impedance of 3 O cm^2 (Fig. 1c).[32] However, these aqueous inorganic acid solutions not only remove Li_2CO_3 but also corrode LLZTO. In response, Guo *et al.* developed anhydrous polyphosphoric acid (PPA) to remove Li_2CO_3 without damaging water-sensitive LLZO. In particular, the formed Li-PPA interlayer not only facilitated the uniform spreading of molten lithium metal but also created a robust electron-blocking shielding to suppress the formation of lithium dendrites.[52]

In addition to acids, other substances such as NH_4F and $LiPO_2F_2$ can also undergo conversion reactions with Li_2CO_3.[53,54] Fei *et al.* devised a general modification strategy to convert pollutants on the surface of LLZTO into LiF and Li_2PO_3F-rich lithiophilic interfaces by performing targeted chemical reactions between $LiPO_2F_2$ and Li_2CO_3/LiOH. The newly formed LiF–Li_2PO_3F interface layer both facilitated the interface wettability between lithium metal and LLZTO and resisted the corrosion of the LLZTO surface by moisture in the air (Fig. 1d).[54]

2.3.2 Introduction of interlayers. Although LLZO exhibits the lithiophilic nature after removing the contaminants and the CCD has been improved, it still cannot meet the requirements of rapid charging/discharging of batteries. To address this limitation, the implementation of an interlayer between the lithium metal and LLZO has been proposed to reduce the interface impedance and suppress lithium dendrites. Li^+ and e^- are transported and exchanged at the interface between the electrode and LLZO during the charge–discharge process. Taking into consideration the Li^+ and e^- transport capabilities of the interlayer, we categorize the interlayers into three models: electron conductive layer, ion conductive layer, and MCL.

(i) Electron conductive layer. Alloying other metals with lithium metal can improve the anode wettability against LLZO,

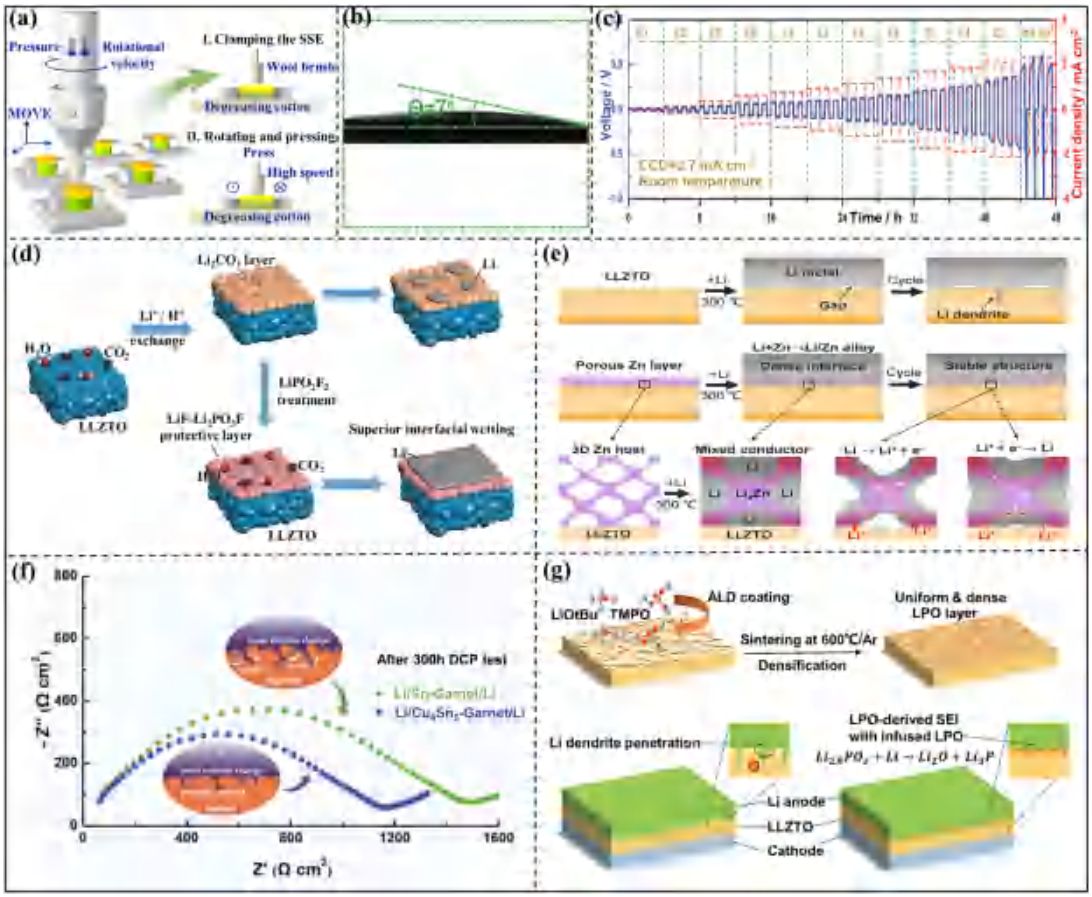

Fig. 1 Strategies of removing Li_2CO_3 and introducing electron/ion conductive interlayers for anode/LLZO interfaces. (a) Schematic of ultraclean LLZTO surface enabled by ultra-high-speed mechanical polishing. Reproduced with permission from ref. 47. Copyright 2022 Elsevier. (b) Contact angle measurement of BM-LLZTO and molten Li metal. Reproduced with permission from ref. 32. Copyright 2023 Wiley-VCH. (c) CCD of the Li|BM-LLZTO|Li cells. Reproduced with permission from ref. 32. Copyright 2023 Wiley-VCH. (d) Schematic illustration showing the *in situ* formation process of the protective Li_2PO_3F-LiF layer on the LLZTO surface. Reproduced with permission from ref. 54. Copyright 2022 Wiley-VCH. (e) Schematics of the LLZTO/Li interfaces, LLZTO@PZL/Li interfaces and the enlarged images of LLZTO@PZL/Li interfaces, which indicate the enhanced kinetics and stable structure of the LLZTO/Li interface during cycling. Reproduced with permission from ref. 61. Copyright 2021 Elsevier. (f) EIS profiles of Li/Sn-garnet/Li and Li/Cu_6Sn_5-garnet/Li symmetric batteries after the direct current polarization test for 300 h. Reproduced with permission from ref. 62. Copyright 2019 American Chemical Society. (g) Schematic diagram of the preparation process of the lithium phosphate layer and its promotion of uniform Li deposition. Reproduced with permission from ref. 65. Copyright 2020 Wiley-VCH.

effectively reducing the lithium metal/LLZO interfacial impedance. Meanwhile, the alloy can enhance the transport kinetics of Li^+ and promote the uniform distribution of Li^+ at the interface. Various metals are introduced into lithium metal to form alloy anodes, such as Mg, Sn, Cu, Sb, Au and Sr.[55–60] Nevertheless, the alloy anode suffers from massive volume expansion during the charging/discharging cycle. To solve this problem, Chen *et al.* coated a 3D porous zinc layer (PZL) onto the surface of LLZTO by magnetron sputtering technology and constructed a 3D Li–Zn alloy layer at the LLZTO/lithium metal interface by heating. This 3D Li–Zn alloy interface's host effect effectively suppressed lithium metal's volume expansion and improved the interface stability between LLZTO and the 3D alloy anode. Li/LLZTO@PZL/Li symmetric cells achieved a high CCD of 2 mA cm^{-2} (Fig. 1e).[61] Although the 3D alloy frame effectively alleviates the volume expansion, it cannot provide capacity due to the inactive frame elements. Besides, the high weight ratio of the inactive frame could significantly reduce the energy density of the SSLMB. Developing a method that can both limit the volume change and reduce the proportion of inactive metals is meaningful. Xia *et al.* developed a thin Cu_6Sn_5 artificial interlayer with a thickness of 50 nm by magnetron sputtering, which could simultaneously suppress volume changes and ensure close contact between the lithium metal and LLZO. In addition, the Cu_6Sn_5 film was very lightweight, and hardly reduced the energy density of the alloy anode. The experimental results indicated that the Cu atom in Cu_6Sn_5 could reduce the volume change of the alloy anode and inhibit the diffusion of Sn. Thanks to the support of the $Li_{2+x}Cu_{1-x}Sn$ frame, the anode remained in close contact with LLZO during the cycles (Fig. 1f).[62]

(ii) Ionic conductive layers. Alloy interlayers have outstanding lithiophilicity and high electronic conductivity, which may

induce lithium dendrites to grow on the lithium metal or deposit inside LLZO. In contrast, the ionic conductive layer with lithiophobicity and electronic insulation can suppress the lithium dendrites because the lithiophobic interlayer with weak bonding to the Li atom promotes the plane Li atom diffusion along the lithium metal/LLZO interface and suppresses the vertical growth of lithium metal.[36,37,63,64] Moreover, the low electronic conductivity of the interlayer also prevents the actual potential of LLZO from dropping to 0 V, thus suppressing lithium metal deposition inside LLZO.

Zhang *et al.* constructed a uniform and dense Li_3PO_4 (LPO) layer on the surface and inside of LLZO through atomic layer deposition (ALD) and a high-temperature annealing process, which could not only improve the air stability of LLZO, but also significantly reduce the interface resistance to 1 Ω cm^2, thus achieving a high CCD of 2.2 mA cm^{-2} at room temperature. Apart from improving the mechanical strength and Li^+ conductivity of grain boundaries, the coated and injected LPO also formed a stable Li^+ conductive and electronically insulated solid electrolyte interface between lithium metal and LLZO, thus eliminating lithium dendrites and preventing high-valence elements from being reduced by lithium metal during long cycles (Fig. 1g).[65] However, the high interface energy between the ion conductive layer and the lithium metal leads to poor interface contact and high interfacial resistance, which needs to be further improved.

(iii) Mixed ionic/electron conductive layers. With the previously discussed interlayers, clearly, it is very hard to construct an interlayer that can both achieve a low interface resistance (lithiophilicity) and a strong dendrite suppression capacity (lithiophobicity). This issue may be solved by combining the lithium alloy and ion conductor to create a MCL. Sun *et al.* deposited a uniform Cu_3N film on the surface of LLZTO pellets, and the Cu/Li_3N MCL was *in situ* formed at the interface between lithium metal anode and LLZTO by reacting molten lithium metal with the Cu_3N film at 200 °C. The interfacial resistance dramatically decreased from 1138.5 to 83.4 Ω cm^2 at 25 °C. The Li_3N matrix in the MCL provided effectual ion-conducting pathways for Li^+, while the well-dispersed Cu nanoparticles guided a homogenous electric field at the interface. The synergistic effect of the external ionic conductivity and internal electronic conductivity relieved the electron attack to LLZTO, thus suppressing lithium dendrite nucleation. The resulting CCD of MCL-protected LLZTO was as high as 1.2 mA cm^{-2}. The batteries exhibited stable cycling over 1000 h with a low overpotential of 30.1 mV under 0.1 mA cm^{-2} (Fig. 2a).[66] Similar interlayers include MgF_2, Al_2O_3, ZnO, Ta_2O_5, SnS, SnS_2, and Al–Si.[67–75]

Not only inorganic substances can react with lithium metal to form a MCL, but organic substances can also transport both lithium ions and electrons. Organic layers can establish good interfacial contact and buffer the volume change of the lithium anode since they are soft and flexible.[78,81] Ren *et al.* developed lithium naphthalenide (Li-Naph(s)) as MCL, which possessed high lithium-ion conductivity of 4.38 mS cm^{-1} and delocalized an electron conductivity of 1.01 mS cm^{-1}, fulfilling the interlayer requirements of rapid ion/electron exchange. The consistent composition of the Li-Naph(s) layer aided in the uniform distribution of the electric field, lowered the interfacial impedance, and inhibited the formation and growth of dendrites. The solid-state symmetrical battery assembled with lithium metal modified with Li-Naph(s) cycled for 1200 h at 0.2 mA cm^{-2}.[77]

The effective contact area of two-dimensional (2D) solid–solid contact between lithium metal and LLZO is limited. Compared with 2D interlayers, three-dimensional (3D) interlayers can greatly enlarge the contact area and reduce the local current density. In order to form a 3D interlayer between lithium metal and LLZO, researchers set their sights on constructing multiple-layer LLZO sheets.[77,82–85] Hu *et al.* prepared porous-dense-porous three-layer LLZO sheets by a tape-casting method and coated it with a layer of uniform and continuous carbon nanotubes (CNTs). These CNTs promoted the immersion of lithium metal into the porous structure, forming an ion-electron conductive Li–C anode. Due to the continuous coating of the CNTs and its seamless contact with LLZO, uniform lithium deposition occurred within porous LLZO. The Li–C/LLZO interface impedance was only 25 Ω cm^2. Symmetrical batteries with Li–C/LLZO enabled long cycling of 200 h at a current density of 1 mA cm^{-2} (Fig. 2b).[86]

In addition to MCL, the interface layer composed of lithium alloy and pure ionic conductive interphase exhibits a more excellent effect of reducing impedance, suppressing lithium dendrites, and improving CCD. Xia and his group prepared AlN interlayer on the LLZTO surface through magnetron sputtering. When AlN was reacted with lithium metal at 400 °C for 15 min, a mixed conductive interphase consisting of Li_xAl alloy particles embedded in a Li_3N network was formed. Then, Xia *et al.* diluted Li_9Al_4 alloy particles into bulk lithium metal by prolonging the annealing treatment time to 120 min, obtaining Li_3N/Al-doped lithium metal interphase. Rapid Li atom diffusion was achieved by the resulting Li_3N/Al-doped lithium metal interphase, which also had an electron-isolating and ion-conductive property. As a result, a high CCD of 2.6 mA cm^{-2} was achieved by Li_3N/Al-doped lithium metal interphase–modified LLZTO. In comparison, a mixed conductive interphase made of Li_xAl alloy particles embedded in a Li_3N network produced a modest CCD of 1.2 mA cm^{-2} (Fig. 2c).[79]

MCL containing gradient components is also of interest to researchers. Goodenough *et al.* constructed the gradient interlayer *via* a self-regulating reaction between lithium metal and AlF_3. Due to the significant difference in the interfacial energy between Li/Li_9Al_4 and Li/LiF (Fig. 2d), a gradient interface layer of LiF–LiAl–Li was formed from top to bottom after the molten lithium metal reacted with AlF_3 (Fig. 2e). The LiAl alloy in the functional gradient lithium anode (FGLA) significantly reduced the interface impedance, and LiF inhibited lithium dendrites. FGLA dramatically reduced the FGLA/LLZTO interface impedance to B1 Ω cm^2 and increased the CCD to 3.0 mA cm^{-2} at room temperature (Fig. 2f).[80] Numerous materials were employed to construct gradient mix ionic/electron conductive layers such as AgF and SnF_2.[76,87] These mix ionic/electron conductive layers are usually generated *in situ* on the surface of the lithium metal, which can realize the seamless connection among the lithium metal, MCL and LLZO. The seamless

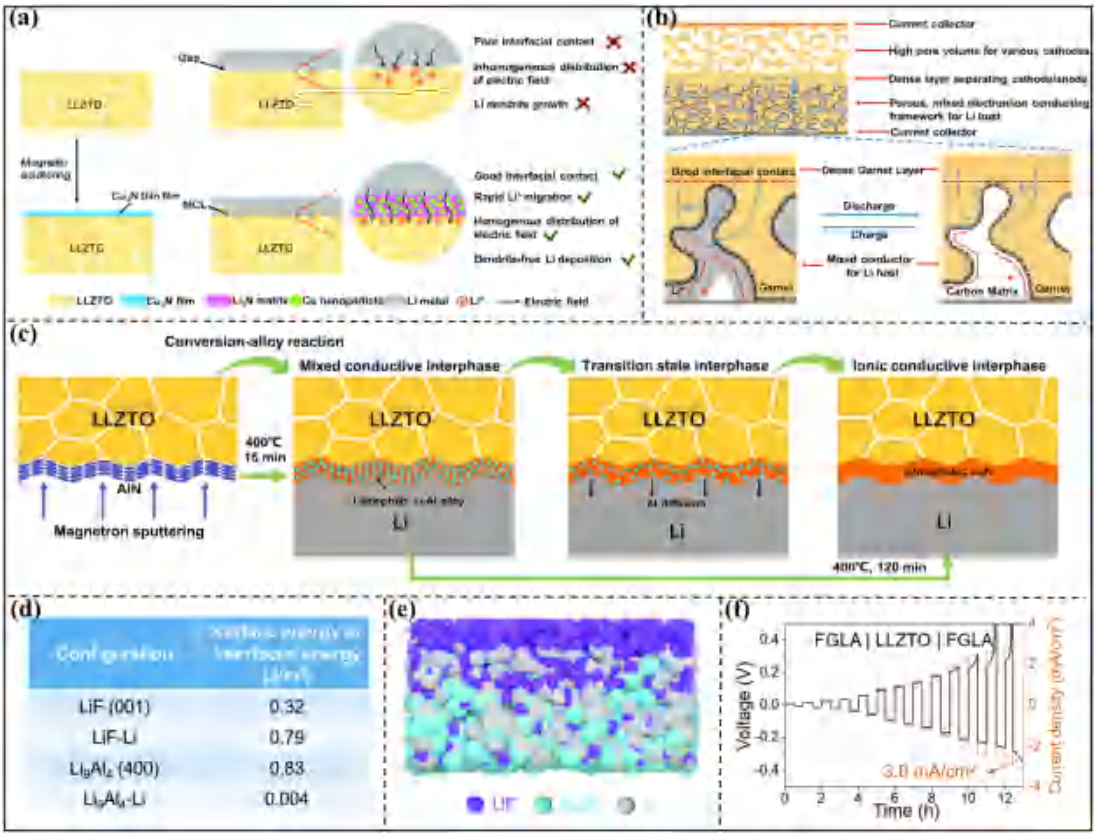

Fig. 2 Mixed ionic/electron conductive layers for anode/LLZO interfaces. (a) Schematic of the MCL-protected LLZTO/Li interface for the dendrite-free lithium metal anode. Reproduced with permission from ref. 66. Copyright 2020 Royal Society of Chemistry. (b) Structure of the porous-dense-porous trilayer garnet framework and working mechanism on the anode side during discharge and charge processes. Reproduced with permission from ref. 86. Copyright 2018 American Chemical Society. (c) Schematics of AlN-modified LLZTO, mixed conductive interphase-modified LLZTO, transition-state interphase-modified LLZTO, and ionic conductive interphase (ICI)-modified LLZTO. Reproduced with permission from ref. 79. Copyright 2022 American Association for the Advancement of Science. (d) Surface energies of LiF (001) and Li_9Al_4 (400), and the interfacial energies of the LiF/Li interface and Li_9Al_4/Li interface. Reproduced with permission from ref. 80. Copyright 2022 Royal Society of Chemistry. (e) Schematic representation of the FGLA. Reproduced with permission from ref. 80. Copyright 2022 Royal Society of Chemistry. (f) CCD measurements of FGLA|LLZTO|FGLA symmetrical batteries. Reproduced with permission from ref. 80. Copyright 2022 Royal Society of Chemistry.

connection between the ion conductive layer and LLZO plays a role in electron isolation and ion conduction while raising the actual potential of the LLZO surface above 0 V and inhibiting lithium metal deposition within LLZO.

We provide a summary of strategies with the aim to reduce interface resistance and its impact on cell performance (Table 1). These strategies have proven to be effective in decreasing the interface impedance to less than 100 O cm^{-2} while increasing the CCD to more than 1 mA cm^{-2}. Moving forward, it is imperative to identify efficient, cost-effective materials and interfacial treatment processes that can meet the demands for large-scale market applications for optimizing the anode/SSE interface.

3. Cathode/LLZO interfaces

The immutability of LLZO causes inadequate physical contact between LLZO and the active/inactive cathode components. On one hand, the cathode/LLZO interface contains numerous voids, which impedes ion transfer and increases resistance. On the other hand, battery cycling exacerbates the deterioration of this poor interfacial contact.[88,89] Aside from poor physical contact, unsatisfactory chemical/electrochemical stability is still a challenge to the cathode/LLZO interface. Li_2CO_3 impurities may be introduced to the cathode/LLZO interface owing to LLZO's chemical instability in air. Additionally, cathode active materials (CAMs) have higher potential than LLZO, which causes electrochemical parasitic processes to occur at the cathode/LLZO interface. Meanwhile, local charge depletion or enrichment is frequently caused by the space charge layer at the cathode/LLZO interface, which may impact charge transport.[90] These problems severely limit the contact stability and ion transport of the cathode/LLZO interface. For a more comprehensive understanding of these issues, the cathode/LLZO interface issues are discussed in this section along with the appropriate solutions.

3.1 Interfacial contact issues and corresponding strategies

Typical methods for solving contact issues include co-sintering techniques, surface coating techniques, soft ionic conductor interlayers, as well as the design of material size and structure.

Table 1 Summary of interfacial resistance, CCD and cycling stability

Strategies	Interfacial resistance (O cm^2)	CCD (mA cm^{-2})	Cycle stability		Ref.
			Current (mA cm^{-2})	Cycle life (h)	
High-speed mechanical polishing	28.15	1.91	0.1	1200	47
			0.3	400	
			1	200	
HCl treatment	26	—	0.2	700	49
HCl-LiF treatment	11.6	1.8	0.1	1400	51
			0.5	1000	
HF treatment	3	2.7	0.1	12 000	32
SnS treatment	5.1	0.9	0.3	800	73
			0.4	700	
Al–Si interlayer	15.0	1.2	0.1	1500	75
			1	800	
Ag-LiF interlayer	5.8	0.75	0.2	600	76
			0.5	130	
Cu_3N interlayer	83.4	1.2	0.1	1000	66
			0.5	400	
MgF_2 interlayer	25	0.65	0.3	1000	67
Al_2O_3 interlayer	8.4	1.0	0.3	1000	69
Ta_2O_5 interlayer	9	2	0.2	5200	72
			0.4	200	
Li-Naph(s) interlayer	131.8	1.7	0.2	1000	77
PAA interlayer	254.5	1.2	0.5	400	78
AlN interlayer	30.3	2.6	0.1	3600	79
			1	600	
AlF_3 interlayer	B 1	3	0.3	670	80
SnF_2 interlayer	56	2.4	0.5	1000	87
			1	300	

3.1.1 Co-sintering technology. Through simultaneous sintering of several phases, co-sintering technology is a promising method to improve interfacial contact significantly. However, during the high-temperature treatment, the CAMs could undergo elemental cross-diffusion reactions with LLZO, producing a highly resistive interfacial second phase.[91,92] Consequently, it is necessary to optimize the co-sintering procedure. For this, the four directions listed below are developed.

(i) Modification of the sintering atmosphere. Moisture and carbon dioxide in the air would react with LLZO to form high-impedance byproducts during the calcination process. Therefore, the harmful gases should be strictly eliminated during the calcination process. Controlling the sintering atmosphere, such as applying pure oxygen atmosphere, is an effective way to reduce interface resistance.[93] However, Kim *et al.* discovered that the interface of LLZO/CAMs cannot be stabilized under a pure oxygen atmosphere. Because Li diffusion from LLZO-Ga to NCM523 occurred at high temperatures under any atmosphere, resulting in the decomposition of LLZO-Ga into $La_2Zr_2O_7$. Furthermore, sintering in N_2 atmosphere caused the reduction of Ni^{2+}/Ni^{3+} in NCM523 and changed LLZO-Ga's cubic phase to a tetragonal one (Fig. 3a).[94] In conclusion, it is difficult to solve the interface problem only by controlling the sintering atmosphere.

(ii) Adjustment of sintering components. Rohlfing *et al.* investigated the influence of the composition on the secondary phase formation. They argued that nickel-rich $LiNi_{0.8}Co_{0.1}Mn_{0.1}O_2$ (NCM811) was more stable than $LiNiCoMnO_2$ (NCM111) when co-sintering with LLZTO. They used spin density difference (SDD) plots to value the stability of materials. The charge state of Ni^{4+} could be clearly seen from the SDD plot where no SDD feature of Ni was observed, indicating that no secondary phase formed (Fig. 3b). The calculations clearly underlined that a cathode material with a low Mn content like NCM811 was more suitable for co-sintering with LLZTO since Mn and Co were easy to exchange with LLZTO's Zr element.[95]

(iii) Shortening the sintering time. Rapid thermal annealing process aids in reducing the sintering time, decreasing parasitic reactions, and achieving good cathode/LLZO interfacial contact.[96,97] The rapid, high-temperature microwave soldering method created by Hu's group could quickly form an intact and continuous V_2O_5 layer surrounding carbon black nanoparticles, resulting in a remarkable 690-time increase in the electronic conductivity of V_2O_5-based solid-state cathodes. Furthermore, the molten V_2O_5-based solid-state cathode was conformally soldered to the LLZO sheet, maintaining a tight interface contact without impurities (Fig. 3c).[97]

(iv) Introduction of additives. Suitable additives and solders can change impurities into an ideal buffer interlayer and lower the sintering temperature. For instance, Wang *et al.* created an all-ceramic cathode/LLZO interface with low resistance utilizing $Li_{2.3}C_{0.7}B_{0.3}O_3$ as an additive. $Li_{2.3}C_{0.7}B_{0.3}O_3$ could melt at 700 1C and then react with Li_2CO_3 formed on both LLZO and $LiCoO_2$ (LCO) to create the $Li_{2.3-x}C_{0.7+x}B_{0.3-x}O_3$ (LCBO) interphase (Fig. 3d). This interphase-engineered battery significantly increased the electrochemical performance in terms of capacity and cycle life (83 mA h g^{-1}, 100 cycles at 0.05C), whereas the battery without the $Li_{2.3}C_{0.7}B_{0.3}O_3$ sintering additive only delivered a low reversible capacity of 35 mA h g^{-1} in the first cycle.[98] A small amount of CAM may also serve as a

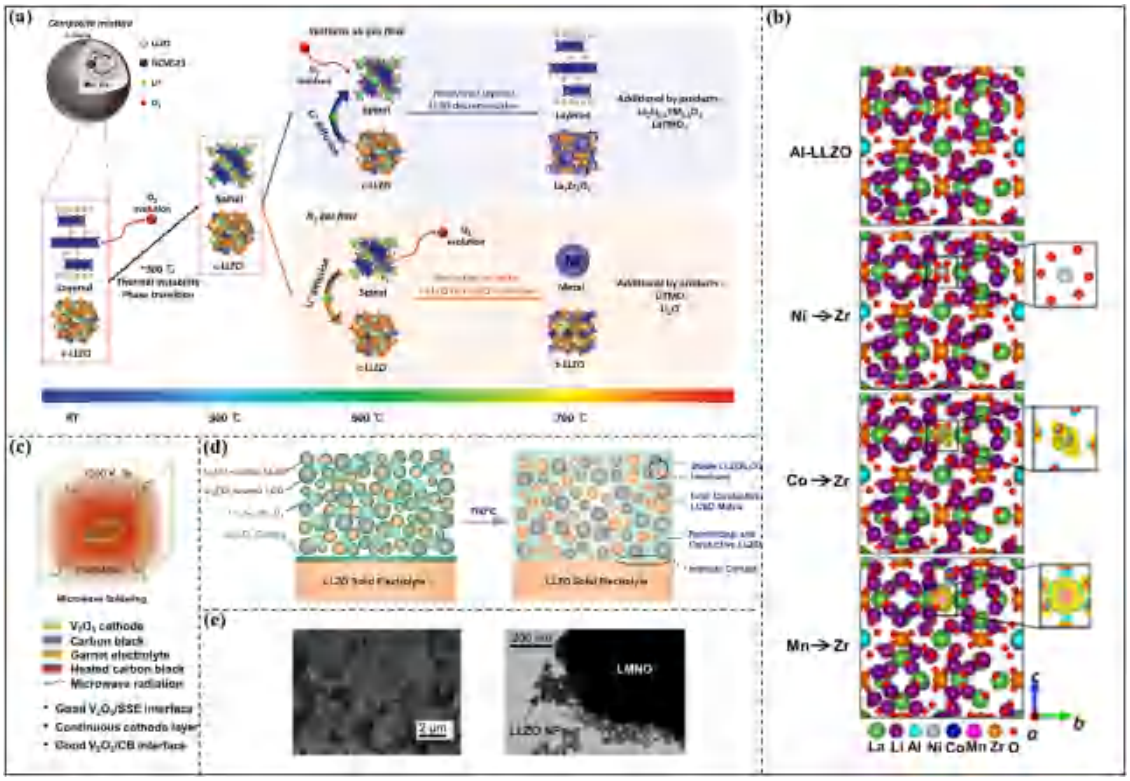

Fig. 3 Influence factors and optimization strategies of cathode/LLZO interfaces. (a) Schematic of crystal structure transition and Li-ion diffusion in the mixture of NCM523 and LLZO-Ga during the co-sintering process under air or N_2. Reproduced with permission from ref. 94. Copyright 2021 Wiley-VCH. (b) Spin density differences for Al-LLZO without and with substitution of Zr atoms with Ni atoms, Co atoms, and Mn atoms. The up- and down-spin electrons are in yellow and blue, respectively. Reproduced with permission from ref. 95. Copyright 2022 American Chemical Society. (c) Diagram of V_2O_5 penetrating the pores between carbon black and garnet electrolytes when heated. Reproduced with permission from ref. 97. Copyright 2020 Elsevier. (d) Schematics of the interphase-engineered all-ceramic cathode/electrolyte interface. Reproduced with permission from ref. 98. Copyright 2018 Elsevier. (e) SEM and TEM images of the LMNO/LLZO mixed powder. Reproduced with permission from ref. 106. Copyright 2022 American Chemical Society.

suitable sintering additive. Wang *et al.* introduced crystalline $LiCoO_2$ into $Li_{6.54}La_{2.96}Ba_{0.04}Zr_{1.5}Nb_{0.5}O_{12}$ (LLBZNO). Due to the synergistic effect of Co^{3+}, Nb^{5+}, and Ba^{2+}, the LLBZNO-3%LCO composite SSE exhibited a high ionic conductivity of 0.28 mS cm^{-1} at 25 1C. Furthermore, owing to minimal element cross-diffusion, the interface resistance of cathode/LLZO reduced from 121.2 O cm^2 to 10.1 O cm^2.[99]

Overall, from the perspective of composition and process, co-sintering technology can powerfully improve interfacial contact while suppressing parasitic reactions at high temperatures through various improved strategies.

3.1.2 Surface coating. Surface coating refers to preparing a protective layer on the surface of the target material. The contact area and ion transport channel between the solid-state cathode and LLZO could be increased by coating the LLZO surface with solid-state cathode or coating the solid-state cathode surface with LLZO. The typical method is to grow a thin-film solid-state cathode on the surface of the LLZO sheet through vapor or liquid methods. Pulsed laser deposition (PLD) was used by Abakumov *et al.* to grow an ultra-thin LCO layer (about 500 nm) on the LLZTO sheet.[100,101] Lee *et al.* developed the spin coating and multi-step heat treatment for the deposition of LCO thin-film cathodes on LLZO particles, ensuring the homogenous deposition of LCO on LLZO particles. With this thin film cathode, an all-solid-state rechargeable battery achieved a high discharge capacity of approximately 100 mA h g^{-1}.[102] Another common approach is to coat the solid-state cathode surface with LLZO through physical/chemical methods such as mechanical ball milling, sol–gel, and flame-assisted ball-mill coating.[103–106] These techniques are effective in adjusting the size of the LLZO layer and guaranteeing the uniformity of the LLZO layer, and the coated cathode exhibits excellent electrochemical performance compared to the pristine one due to the improvement of cathode/electrolyte interfacial contact.[107] Laine *et al.* used LLZO nanopowders (NPs) to modify the $LiMn_{1.5}Ni_{0.5}O_4$ (LMNO) cathode. The LLZO NPs were well covered on the surface of the LMNO cathode by ball milling without generating apparent agglomeration (Fig. 3e).[106]

3.1.3 Introduction of soft ionic conductors. Another typical approach to improve the interfacial contact is to add soft ionic conductors, such as liquid electrolytes, ionic liquids, plastic crystal electrolytes, polymer SSEs, and *in situ* gel electrolytes at the solid-state cathode/LLZO interface.[108–112] In terms of cost and processing ease, liquid electrolytes are the most advanced soft ionic conductors. However, they frequently react with

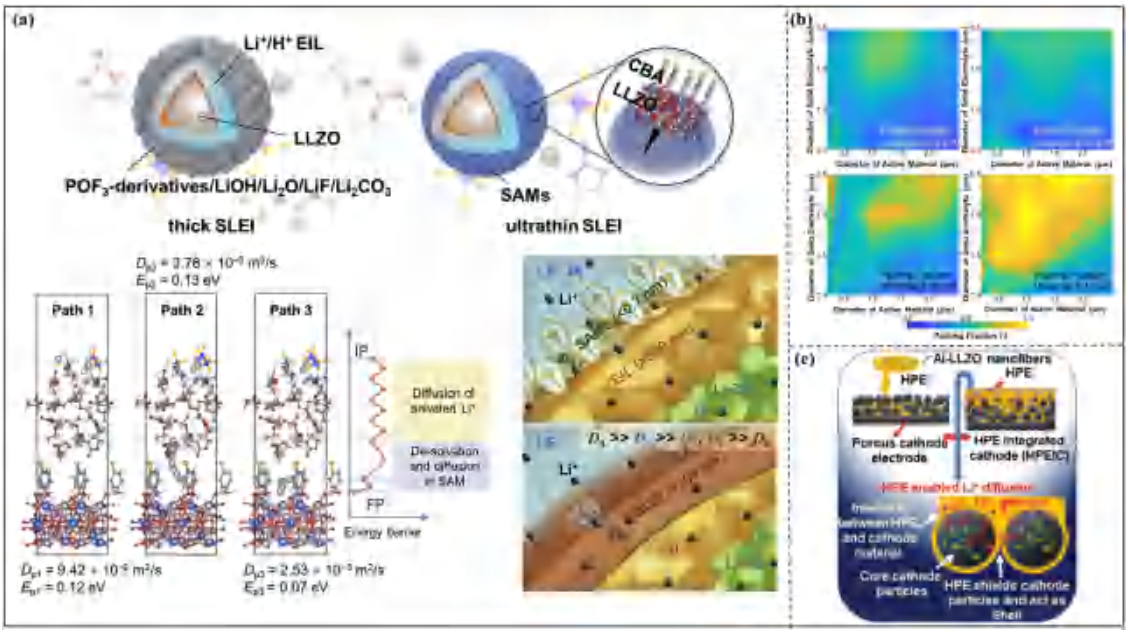

Fig. 4 Intrinsic characteristics and optimization strategies of cathode/LLZO interfaces. (a) Schematics of the surface composition of LLZO in liquid electrolytes (LEs) with or without an ultrathin SAMs protection layer (top). Stimulated diffusion process and migration energy barrier profile for Li^+ diffusion (bottom-left corner). IP indicates initial position. FP indicates final position; Schematics of Li^+ migration from LE to LLZO sheets with or without the SAM protection layer (bottom-right corner). Reproduced with permission from ref. 108. Copyright 2022 Elsevier. (b) Final packing fraction of the SSE in the vicinity shell for a range of cathode active material primary particle sizes and initial mean diameters. Reproduced with permission from ref. 121. Copyright 2021 Elsevier. (c) Design of interface-based core–shell and hybrid polymer electrolyte (HPE)-enabled Li-ion diffusion. Reproduced with permission from ref. 123. Copyright 2022 Wiley-VCH.

LLZO, decreasing the energy density and thermal stability of the battery. LLZO degradation mechanism was identified by Luo *et al.* They found that the protic impurities in the fresh liquid electrolyte should be the root cause for the Li^+/H^+ exchange. The Li^+/H^+ exchange would be accelerated when LiOH captured CO_2 to form Li_2CO_3. Self-assembled monolayers (SAMs) were developed to protect LLZO from liquid electrolytes. SAMs were massive ordered fields of spontaneously assembled molecules that develop through surface adsorption. To grow SAMs on the LLZO surface, the authors utilized acidic molecular solutions containing 4-chlorobenzoic acid (CBA). This protective layer prevented the LLZO surface from absorbing organic decomposition products of the liquid electrolyte (Fig. 4a). With the modification of SAMs, a liquid–solid hybrid battery improved by over 39% in specific energy.[108] Compared to liquid electrolytes, polymer SSEs often have superior electrochemical and thermal stability. Moreover, polymer SSEs can provide an effective buffer against stress build-up.[111,113] However, polymer SSEs still have a low ionic conductivity, and more works need to be done to increase their oxidative stability. *In situ* gel electrolytes provide better stability while preserving intimate contact in comparison to liquid electrolytes and polymer SSEs.[114] Zhao *et al.* thermally polymerized a new *in situ* gel electrolyte based on PMMA that could combine LLZO with the cathode and greatly simplify the production of SSEs. After optimizing, the SSLMB exerted a capacity retention of 82.6% after 100 cycles at room temperature.[115] In general, the soft ionic conductors show obvious positive effects on optimizing the interface, and future research should concentrate on further improving their chemical stability. In addition, the sulfur cathode is also unstable against LLZO. The development of the interface buffer layer is expected to make the application of LLZO in lithium-sulfur batteries possible. Fichtner *et al.* designed a gel interlayer based on ionic liquids to improve the interfacial properties. LLZO could successfully confine polysulfides to the cathode and effectively prevent the dissolution of polysulfides to the lithium metal side. The lithium-sulfur SSB delivered an initial discharge capacity of 1360 mA h g^{-1} and a discharge capacity of 570 mA h g^{-1} after 100 cycles.[116] Wachsman *et al.* developed an innovative gel polymer buffer layer to enhance the stability of the sulfur cathode/LLZO interface. The composite interfacial layer formed by the gel polymer layer and ZnO layer effectively promoted the stability of the cathode–electrolyte interface. By adopting a thin bilayer LLZO architecture (dense/porous) as a SSE and incorporating a high sulfur loading of 5.2 mg cm^{-2}, the lithium-sulfur battery demonstrated a high initial discharge capacity of 1542 mA h g^{-1} and maintained an average discharge capacity of 1218 mA h g^{-1} with 80% capacity retention over 265 cycles.[117]

3.1.4 Design of size and structure. It is common knowledge that using smaller LLZO and CAMs will increase the effective contact area and decrease the ion diffusion path. However, the reduced particle size also promotes parasitic reactions, and the additional boundaries may also have adverse effects on ion diffusion.[118–120] Therefore, achieving a high ion transport rate and good interfacial stability requires the proper size ratio of

CAM/LLZO particles. Belharouak *et al.* used primary and secondary active material particles of different sizes to simulate the solid-state cathode packing model (Fig. 4b), and the particle size ratio of CAM/LLZO was optimal between 0.3 and 0.4.[121]

Reasonable structural design not only increases the effective contact area but also forms a continuous ion/electron transport network within the solid-state cathode. The structures of composite cathodes are commonly constructed by template or infiltration methods. The template method generally involves injecting a cathode precursor and LLZO precursor into a polymer template and then removing the excess template by calcination to form a 3D transport channel.[122] The percolation method involves the gradual penetration of the LLZO slurry from the upper layer into the internal void of the CAM-casted cathode (Fig. 4c)[123] or gradual penetration of the CAM-based slurry into the LLZO-casted cathode.[124] Other contemporary methods of structural manufacturing are also available. Tucker *et al.* designed a LLZO-supported electrode and designed the engineering structure using phase inversion (PI) and high shear compaction (HSC) processes. A free-standing LLZO with the highest porosity (75.4%) was obtained after sintering. Then, the NMC cathode suspension was dropped into porous LLZO to form the LLZO-supported cathode.[125] In addition, Rohlfing and colleagues used continuous layer casting to create the microstructure of a composite cathode. In the composite cathode, the concentration gradient of the CAMs and electrolyte was opposite. Owing to the optimized microstructure, the discharge capacity of the free-standing composite cathode increased to 2.8 mA h cm^{-2}, which was 99% value of the theoretical capacity.[126]

3.2 Chemical/electrochemical instability and optimization strategies

Chemical instability frequently causes degradation of the cathode/LLZO interface. Electrochemical instability would cause parasitic reactions. During battery cycling, parasitic reactions accompanied by rapid electron transfer are serious.

In view of chemical instability, the most significant issue is that LLZO is unstable in the presence of air. Due to the formation of Li_2CO_3 byproducts on the LLZO surface, high resistive interface could form at the LLZO/cathode interface. Different approaches, like rigorous management of the raw materials and atmosphere during the LLZO manufacturing process, have been proposed for eliminating Li_2CO_3. At every stage of the production and storage process, it is crucial to strictly manage the amount of CO_2 and H_2O in the environment. Bilge *et al.* discovered that removing CO_2 and minimizing H_2O (g) during sintering could produce good contact at the cathode/LLZO interface without generating a second phase, which was further validated by comparing DG (T, P_{gas}) in various environmental atmospheres (Fig. 5a).[93]

Because the cathode material's reactivity with LLZO depends on a number of variables such as the cathode active/inactive material's components, the crystallinity of CAMs, and the polarization potential, the issue of electrochemical instability is complex. Among the commonly used CAMs, $LiMn_2O_4$ and $LiFeO_4$ had a higher reactivity with LLZO. $LiCoO_2$ was relatively stable against LLZO, but it still experienced irreversible electrochemical decomposition at the $LiCoO_2$/LLZO contact points when the voltage was above 3 V.[127] The electrochemical stability was also influenced by LLZO's crystal structure. $La_2Zr_2O_7$ and other Li-poor phases were produced when LLZO single crystals disintegrated at 4.1–4.3 V *vs.* Li^+/Li.[128] In a solid-state cathode, the electrochemical reaction involves interfacial ion/electron transport between the CAMs, LLZO, and the conductive agents.[129,130] Electron transfer can be sped up by using carbon conductive additives to lower the electrodes' contact resistance.[131] However, the carbon conductive additives reacted with LLZO and yielded byproducts such as CO_2 or Li_2CO_3.[132] Therefore, Brezesinski *et al.* studied the electrochemical stability between different conductive agents and LLZO. Compared to Ketjen black and Super P, vapor-grown carbon fiber (VGCF) was more successful in controlling interfacial parasitic reactions.[133] The PVDF binder played a role in improving the solid-state cathode's ionic conductivity, strength, and electrochemical stability. The solid-state cathode's electrochemical stability dramatically increased when PVDF content was raised to 7 wt%. The ionic conductivity, however, declined when the amount of binder was continuously increased.[134]

Transforming intermediate layers created by parasitic reactions into novel materials with high ionic conductivity is an inventive way to address the chemical/electrochemical problem of the cathode/LLZO interfaces. For instance, Zhang *et al.* presented an ''interfacial homogeneity'' technique that allowed Li_2CO_3 layers to be *in situ* converted into $LiCoO_2$ by reacting with Co_3O_4 (Fig. 5b). The formed $LiCoO_2$-LLZTO@$LiCoO_2$ composite cathode kept 81% of its initial capacity after 180 cycles at 0.1C when used in SSLMBs.[135] Additionally, artificial interlayers made of a variety of material components have been constructed between cathodes and electrolytes. The artificial interlayers generally include lithium-containing oxides (Li_3BO_3, Li_2SiO_3, and LiH_2PO_4), and oxide materials (Nb_2O_5 and Al_2O_3) that can subsequently be lithiated during electrochemical reactions.[136–141] For example, introducing an *in situ* lithiated Nb_2O_5 layer at the interface of LLZO and $LiCoO_2$ reduced the charge transfer resistance to approximately 50 O cm^2.[139] Ceder and colleagues developed a computational framework concentrating on the ionic conductivity and electrochemical/chemical stability of Li-containing materials. In this research, polyanionic oxides such as LiH_2PO_4, $LiTi_2(PO_4)_3$, and $LiPO_3$ were found to have the best qualities. (Fig. 5c).[138] Similarly, Mo *et al.* provided detailed guidance diagrams for selecting potential compounds that could stabilize the LLZO/NMC interface. They studied the stability between LLZO and the entire Li–M–O ternary composition space (cations M = B, C, N, Al, Si, P, Ti, V, Cr, Zr, Nb, Mo, Zn, Ga, Ge, Ta, or W). The decomposition energy E_d of each composition with LLZO was illustrated by a heatmap of the Li–M–O Gibbs ternary diagram (Fig. 5d). The compositions which were stable with LLZO showed a small magnitude of $|E_d|$ o 0.05 eV $atom^{-1}$ in the heatmaps. It can be seen that many systems with nonmetal M cations exhibited narrow stable compositional space, indicating poor stability

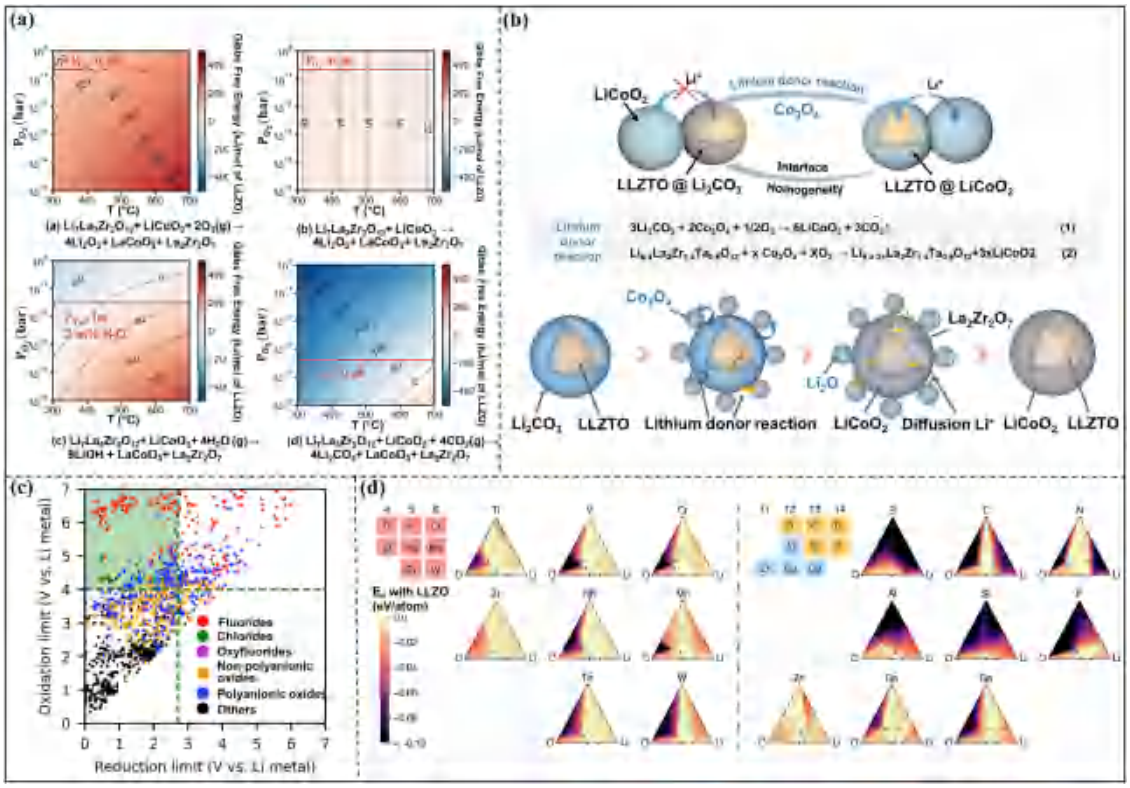

Fig. 5 Design of transition layers for cathode/LLZO interfaces. (a) Gibbs free energy, DG (T, P_{gas}) (kJ mol^{-1} of LLZO) calculated between LLZO and fully lithiated $LiCoO_2$ in different reactions. Reproduced with permission from ref. 93. Copyright 2022 Wiley-VCH. (b) Schematic illustration of the solid-state reaction process of transforming LLZTO@Li_2CO_3 into LLZTO@$LCoO_2$. Reproduced with permission from ref. 135. Copyright 2020 Springer Nature. (c) Electrochemical and chemical stability screening results. Reproduced with permission from ref. 138. Copyright 2019 Elsevier. (d) Heatmaps of the chemical stability of Li–M–O (M = B, C, N, Al, Si, P, Ti, V, Cr, Zr, Nb, Mo, Zn, Ga, Ge, Ta, or W) with LLZO. Reproduced with permission from ref. 142. Copyright 2021 Elsevier.

with LLZO. In contrast, the material systems of Li–Ti–O, Li–Zr–O, Li–Ta–O, Li–V–O, Li–Ga–O, Li–Ge–O, Li–Sn–O, Li–Cr–O, Li–Mo–O, and Li–W–O possessed a wide stable composition region, suggesting that these materials had the potential to serve as coating layers due to their excellent stability with LLZO.[142]

4. Interface within LLZO-based SSEs

The LLZO-based SSEs can mainly be divided into two categories: LLZO sheets and LLZO/polymer composite membranes. It is convenient to assemble SSBs directly using LLZO sheets, but the rigid characteristic of LLZO sheets limits their further application. Combining LLZO with polymers is a promising approach. LLZO have high mechanical strength and ion conductivity, while polymer SSEs have better flexibility and can improve interfacial contact. Therefore, compared to individual LLZO sheets or polymer membranes, LLZO/polymer composite membranes have comprehensive advantages in ion conductivity, thermal stability, and flexibility.[143–145]

4.1 Interface within LLZO sheets

The bulk phase ion conductivity and grain boundary ion conductivity of LLZO both have an impact on the material's total ion conductivity. The grain boundaries are more reactive to yield byproducts than bulk grains, which raises the grain boundary impedance and prevents ion migration. To solve this problem, densification of electrolytes to reduce grain boundaries and defects, increment of the ion migration rate at grain boundaries, and improvement of component purity to reduce parasitic reactions are performed.

4.1.1 Densification of LLZO sheets. The standard method to produce LLZO sheets involves pressing the mother powder into green sheets and sintering them to yield LLZO sheets.[146–148] The sintering procedure, as well as the components of the mother powder, is intimately related to the densification procedure. Therefore, researchers generally adjust the densification effect through these two pathways.[149]

(i) Optimization of the sintering process. Ye *et al.* used an ultrafast sintering method based on CO_2 laser scanning to prepare LLZTO. A LLZTO film could be quickly densified in 1 s with the help of a heating table (Fig. 6a).[150] Recently, Joule heating was developed to control grain growth. By using the Joule heating technique, the particle size distribution of LLZO was discovered to be essentially identical before and after sintering, whereas defects (such as voids and gaps) and impurities were successfully eliminated.[151]

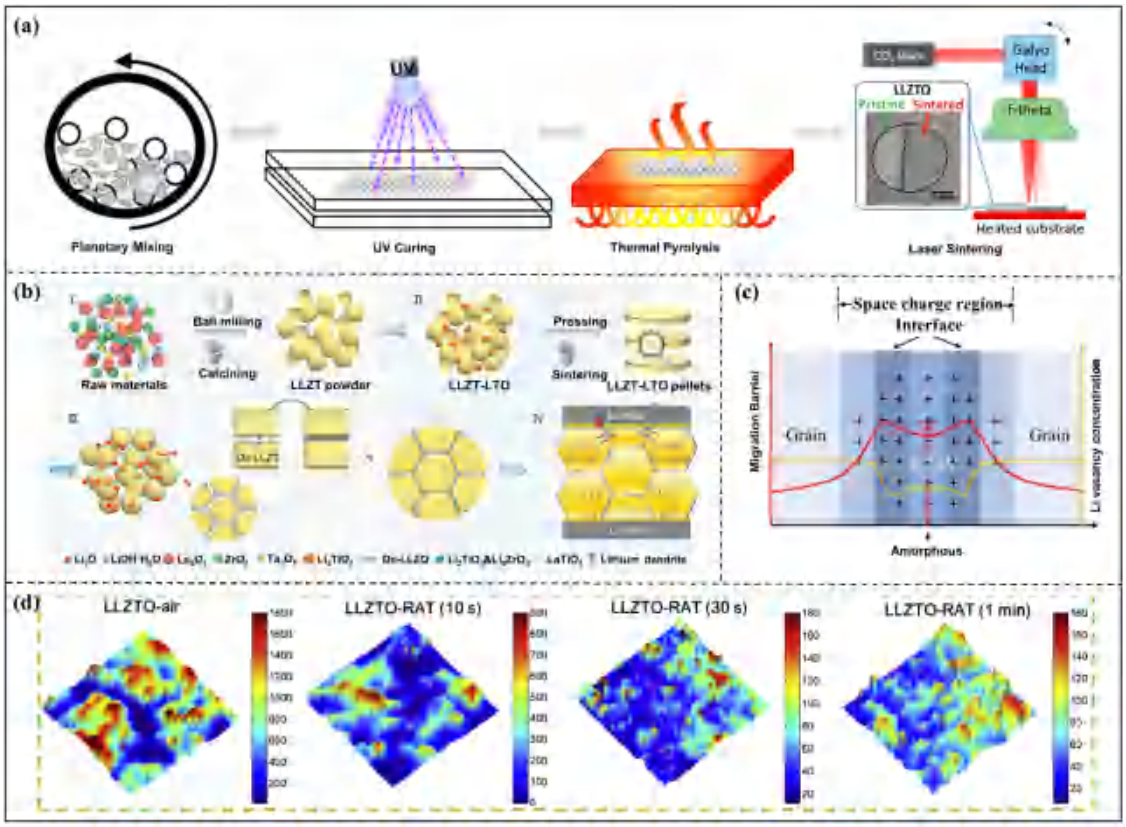

Fig. 6 Influence factors and optimization strategies of interfaces within LLZO sheets. (a) Schematic diagram of the preparation of dense LLZTO by laser sintering. Reproduced with permission from ref. 150. Copyright 2022 American Chemical Society. (b) Schematic illustration of the formation of LLZT-LTO ceramics and the roles of the LTO modification. Reproduced with permission from ref. 152. Copyright 2022 Wiley-VCH. (c) Illustration of the migration barrier and Li vacancy concentration at the grain boundary with amorphous domains. Reproduced with permission from ref. 155. Copyright 2020 Springer Nature. (d) Raman mappings of the aged LLZTO and LLZTO with different acid treatment time periods. Reproduced with permission from ref. 49. Copyright 2019 Elsevier.

(ii) Introduction of additives. The phenomenon of rapid grain growth is known as abnormal grain growth. It can weaken the mechanical properties and reduce the density of LLZO. Fortunately, novel additives can suppress this phenomenon. For instance, Wen *et al.* developed an *in situ* grain boundary modification technique based on the interaction between Li_2TiO_3 (LTO) and Ta-substituted LLZO. Because the generated second phase played a pinning role and prevented the migration of grain boundaries, the formation of $LaTiO_3$ and a small amount of LTO/Li_2ZrO_3 at the grain boundaries suppressed abnormal grain growth (Fig. 6b). This led to a high-performance LLZO sheet with a high CCD of 1.8 mA cm^{-2} and long cycling stability up to 2000 h at 0.3 mA cm^{-2}.[152] Similarly, additives such as La_2O_3[153] and Li_2WO_4[154] can inhibit abnormal grain growth.

4.1.2 Adjustment of the crystallinity of grain boundaries. The properties of the space charge layer at the grain boundaries can vary as a result of different crystallinities. According to Xiang *et al.*, the amorphous domains at the grain boundaries created additional vacancies for Li^+, raising the ionic conductivity of LLZO to 0.6 mS cm^{-1}. This occurrence suggested that adjusting the crystallinity of LLZO could significantly enhance Li^+ migration (Fig. 6c).[155] Designing stable amorphous grain boundaries is an important subject since the amorphous structure is generally unstable. Amorphous LLZO electrolytes with high stability were produced *via* a low-temperature ceramic technique invented by Rupp and colleagues. Furthermore, this low-temperature synthesis technique considerably minimized the parasitic reactions that would take place at high temperatures.[156] In short, changing the crystallinity of grain boundaries is fascinating because it may fundamentally alter the conventional ion conduction mode, considerably increasing the ion conductivity without sacrificing stability.

4.1.3 Component purification. Crucible contamination and Li^+/H^+ exchange would produce phases in addition to the cubic LLZO phase. Purifying the LLZO component is possible with suitable doping agents. In dual-doped $Li_{6.05}La_3Ga_{0.3}Zr_{1.95}Nb_{0.05}O_{12}$, it was found that the doping agents Ga and Nb preferred to occupy the Li position and the Zr site, respectively. Air stability and interfacial resistance were significantly improved in $Li_{6.05}La_3Ga_{0.3}Zr_{1.95}Nb_{0.05}O_{12}$.[157] Hydrophobic compounds such as LiF and Li_3PO_4 are frequently employed as additives to hinder the production of Li_2CO_3.[158,159] A versatile and quick acid treatment approach was suggested by Sun

et al. To thoroughly eliminate surface Li_2CO_3, the aged LLZTO (LLZTO stored in the air) particles were submerged in a robust HCl solution. Raman signals verified the cleaning effect of fast aid treatment on Li_2CO_3 (Fig. 6d).[49] Integrating advanced purification methods with the battery assembly process will be more efficient and promising in the future.

4.2 Interface within composite polymer electrolytes

The ion transport properties within the composite polymer electrolyte (CPE) interface are dependent on several factors including content, morphology, chemical stability, and coordination effect of the ligand structure.

4.2.1 Adjustment of the content. Ion migration at the interface within the CPE is significantly influenced by the ion transport style, which is affected by the percentage of various components.[160] The CPEs can be divided into two categories: ceramic in polymer (CIP) and polymer in ceramic (PIC), with LLZO ratios ranging from low to high. These different types of CPEs have different pathways for ion transport. According to Hu and colleagues, there were typically two percolation thresholds for PIC with the LLZO content above 80%: one was the long interconnection of the ceramic particles themselves, and the other was the interconnection of the ceramic and polymer interfaces. The polymer phase was typically dominant in lithium-ion transport for CIP with the content of LLZO below 20–30%. The size of the particles and the degree of mixing between the components are two criteria that significantly influence the ion migration paths.[161] LLZO fillers could adjust the degree of crystallinity of the polymer. Polyethylene oxide (PEO) is widely used in CPE because it exhibits good solubility with lithium salts.[162] Rettenwander *et al.* observed that the addition of 10 wt% LLZO filler decreased the degree of crystallinity of PEO, while 20 wt% of LLZO filler increased the degree of crystallinity of PEO. By adjusting the degree of crystallinity, they achieved a high-performance SSLMB with a high CCD of 1 mA cm^{-2}.[163]

However, despite substantial advancements in ion conductivity, CIP electrolytes typically show low modulus and penetrability that may cause short circuits in SSLMBs, severely impeding their practical application. PIC electrolytes show a higher mechanical strength. Although PIC electrolytes can more efficiently manage electrode expansion, their ability to operate with lithium metal at room temperature is constrained by the weak flexibility. Therefore, for the sake of mutual complementation, it is highly desirable to combine PIC and CIP electrolytes. A sandwich-type composite electrolyte (SCE) with a flexible CIP outer layer and a high mechanical strength PIC interlayer was thoughtfully created by Sun *et al.* This SCE with graded LLZO particles successfully suppressed lithium dendrite and possessed good interfacial contact with electrodes.[164]

4.2.2 Adjustment of morphology and structure. Local agglomeration and uneven dispersion could occur if the CPE contains too much LLZO fillers, which slows the movement of Li^+ at the interface and results in poor Li^+ migration.[165,166] Furthermore, despite the fact that LLZO particles are evenly and randomly distributed throughout the polymer matrix, it is still difficult to create long, uninterrupted Li^+ transport pathways. Ion movement can be sped up and the agglomeration issue can be resolved by designing distinctive morphological structures for LLZO. As a result, large–surface area LLZO nanowires, nanosheets, and 3D nano frameworks have been constructed. By using a bottom-up technique, Ci and colleagues created lamellar Al-doped LLZO and laminated it with PEO. The lamellar structure provided a continuous interface between the fillers and the polymer matrix, which ensured rapid diffusion of the lithium ions.[167] Chao *et al.* created a CPE fiber network. In order to create a continuous path, they first reinforced the LLZTO fiber network with PAN (polyacrylonitrile) before homogeneously dispersing the PAN/LLZTO fiber network into the polyethylene oxide (PEO) polymer matrix.[168] However, due to the brittleness of the ceramic network, common preparation methods like electrospinning have limitations when it concerns the mechanical properties of the various structural networks based on ceramics. Using polymer-reinforced ceramic fibers is an effective way. For instance, LLZO nanoparticles were electrostatically spun onto PVDF polymer nanofibers to create a three-dimensional (3D) network by Zhang *et al.* (Fig. 7a). The created lightweight, continuously interwoven LLZO-reinforced 3D network had an electrochemical stable window of 5.02 V at 50 1C and a high ionic conductivity of 0.1 mS cm^{-1} at 50 1C.[169] Dispersing LLZO fillers into a 3D polymer networks is also a useful strategy. Through an *in situ* polymerization reaction, LLZTO and 3D PAN nanofibers were combined to create a CPE. The CPE provided a high ionic conductivity of 2 mS cm^{-1}, a lithium transfer number of 0.5, and a mechanical strength of 2.85 MPa.[170] In addition to PVDF and PAN, polyimide (PI) is also a common framework material. For example, a 3D fiber network–reinforced CPE was mainly composed of a solid porous PI film matrix, while LLZTO nanoparticles, lithium salts, and polyvinylidene fluoride (PVDF) polymers were used to fill the matrix. The 3D structure of the PI fiber network could maintain uniform dispersion of LLZTO in PVDF.[171,172]

CPEs have received fresh inspiration from a few intricately constructed structures. In the above-mentioned PIC electrolytes, some polymers can be viewed as ''additives'' to improve the toughness and ion-transport capacities of the bulky ceramic. For instance, a flexible LLZO-based CPE membrane with gaps bridged by styrene-butadiene copolymer (SBC) was created by Hu *et al.* The top and bottom of each square electrolyte chip in the CPE membrane were exposed, promoting the rapid transport of Li^+ in the direction perpendicular to the membrane. Meanwhile, the film had a high ductility of 220% and a ultimate tensile strength of 5.12 MPa (Fig. 7b).[173] CPEs with multiple layers show great promise.[174] An asymmetric bilayer CPE was manufactured by an *in situ* polymerization process, which incorporated a ceramic-rich layer on the anode side and a polymer-rich layer on the cathode side through selective adsorption by glass fiber (GF) separators (Fig. 7c).[175] In order to effectively combine rigidity and flexibility, a suitable structural design is undoubtedly necessary to take full use of CPEs' performance.

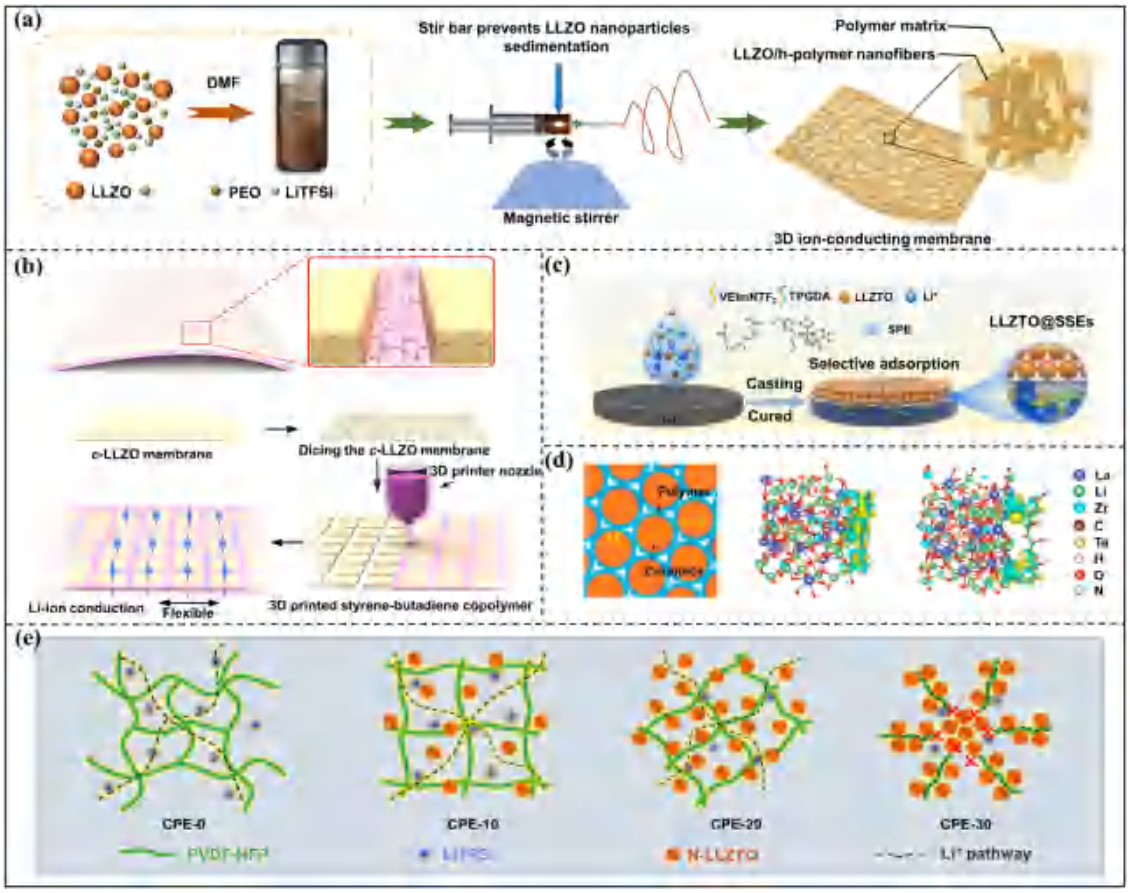

Fig. 7 Optimization strategies of interfaces within composite polymer electrolytes. (a) Schematic diagram of the preparation of the composite polymer electrolyte with LLZO/h-polymer nanofibers. Reproduced with permission from ref. 169. Copyright 2021 American Chemical Society. (b) Schematic diagram of the methodology for the fabrication of a flexible c-LLZO membrane. Reproduced with permission from ref. 173. Copyright 2019 American Chemical Society. (c) Schematic illustration of the functional effect of GF and LLZTO on Li-metal batteries. Reproduced with permission from ref. 175. Copyright 2022 Elsevier. (d) Schematic illustration of the interparticle Li^+ transport in the bulk of the composite electrolyte and calculated CDD at the heterointerface of LLZTO/d-PAN and LLZTO/PAN. Yellow and blue iso-surface represents electron accumulation and depletion regions, respectively. Reproduced with permission from ref. 180. Copyright 2021 American Chemical Society. (e) Schematic diagram of CPE membranes and the paths of ion transport. Reproduced with permission from ref. 181. Copyright 2021 American Chemical Society.

4.2.3 Improvement of the stability of the composite polymer electrolyte. The stability between the constituents of CPEs needs to be taken into account throughout the entire process from production to application because it is a highly complicated system involving inorganic ceramic electrolytes, organic polymers, solvents, and lithium salts. It is important to note that the Li_2CO_3 impurity issue of LLZO still exists in CPEs. In addition, because the functional groups on the surface of LLZO can trigger polymerization, there exist instability issues between the components of the CPEs.

The passivated Li_2CO_3 layer has been demonstrated to inhibit interfacial ion transport and lower carrier concentrations within the CPE. The Li_2CO_3 layer lowers the electropositivity of the LLZO particles, decreasing their ability to bind the anion of the lithium salt. To avoid these problems, Li_2CO_3 must still be taken off the LLZO surface (section 4.1.3).

Mild and stable organic solvents are needed for CPE membrane production. Huang *et al.* discovered, however, that all of the solvents interacted with the LLZO electrolytes *via* Li^+/H^+ exchange, and the degree of reaction depended on the solvent acidity. Due to the hydroxyl groups, alcohol, acetone, and N-methyl pyrrolidone were acidic. This would cause a violent reaction and alter the lattice characteristics of LLZO electrolytes. Ether compounds and saturated aliphatic hydrocarbons with low acidity were relatively stable against LLZO electrolytes.[176]

The stability of LLZO against the polymer must also be taken into consideration. In a CPE of LLZO and polyethylene glycol, LiOH on the surface of the LLZO initiates the polymerization reaction of polyethylene glycol.[177] Competitive coordination structure introduction can minimize contact instability between LLZO and the polymer. For example, Zhang *et al.* suppressed the reactivity of succinonitrile (SN) and LLZO by utilizing the coordination competition between the nitrile groups of PAN and SN with LLZO. In essence, the mutual promotion mechanism was that SN could improve the Li^+ conductivity of PAN, while PAN could protect SN from aggregation. As a result, a long lifespan of over 500 cycles and a high discharge capacity (163 mA h g^{-1} at 0.2C) were achieved.[178] The

interfacial stability in CPEs is easily overlooked in electrolyte design. Besides, it is necessary to study the stability issue in more microscopic aspects.

4.2.4 Enhancement of the interaction between LLZO and the polymer. The surface energy gap between LLZO and the polymer can block the Li^+ transport path. It was found that the interface between the Al-doped LLZO and the PEO–$LiClO_4$ electrolytes had an obvious space charge layer, causing a highly resistive interface.[179] Fortunately, enhancing the interaction between LLZO and polymers is beneficial for improving ion transfer at the interface within the CPE. Xin *et al.* found that the Li^+ dissociated from lithium salt was trapped by the C Q C bond of the PAN polymer, and proved that the coordination of Li^+ by the LLZO surface groups and the groups on the polymer chain played an important role in increasing the ionic conductivity of the CPE (Fig. 7d).[180] Based on Lewis acid–base theory, Ma *et al.* introduced nano-sized LLZTO to the PVDF-HFP substrate to activate the Li^+ coordination between PVDF-HFP and nano-sized LLZTO, thus promoting lithium salt dissociation and then increasing the Li^+ carrier density (Fig. 7e).[181] Overall, suitable chemical coordination can significantly improve the binding between LLZO and polymers, forming high-speed ion transport channels.

5. Comprehensive research tools

As mentioned above, due to the inherent nature of LLZO, there is a problem of poor contact in multiple interfaces inside the battery. We introduced targeted strategies in the former sections for the above-mentioned issues, and there are also some powerful tools to assist us in gaining a deeper understanding of various interfaces in LLZO-based batteries. Advanced characterization techniques and modeling prediction methods are important foundations for proposing effective strategies. The development of characterization technology for SSLMBs enables us to analyze data in a fundamental perspective. Constructing interface modeling greatly narrows the gap between experimental data and computational predictions. In addition, from the perspective of engineering practice, the problems based on battery interfaces in the practical process have been re-examined, and the design of materials and the regulation of battery stress need to be considered.

5.1 Advanced characterization techniques

In situ detection of solid–solid interfaces is a great challenge. Due to the limitations in signal acquisition depth, traditional characterization tools are difficult to achieve high-resolution and direct observation of SSLMBs. Fortunately, with the development of technology and equipment, there are various non-destructive *in situ* techniques to observe solid/solid interfaces including *in situ* SEM observations,[182] X-ray computed tomography,[183] operando neutron depth profiling,[184] and atomic force microscopy.[185] Yang *et al.* traced and monitored the Au/LLZO interface by *in situ* SEM technique, and found that the intrinsic defects of poly-crystalline electrolytes such as pores, grain boundaries, and impurities were the critical factors that caused non-uniform Li deposition. It emphasized the importance of preparing uniform and dense LLZO electrolytes.[182] Winter *et al.* synthesized a novel enhanced CPE using cross-linked PEO–LiTFSI–Pyr_{14}TFSI and LLZO. Combining conventional laboratory techniques and non-destructive synchrotron X-ray tomography, they investigated the synergistic effect of membrane components on homogeneous lithium deposition/dissolution. The X-ray tomography revealed no gap or cavity at the CPE/lithium metal interface, which further suggested an intimate contact between the electrodes and the CPE.[186] Using a combination of advanced techniques including valence-electron energy loss spectroscopy (valence-EELS) in *in situ* high-resolution electron microscopy and spherical aberration-corrected electron microscopy, Chi *et al.* explored the growth mechanism in lithium dendrite inside LLZO and found that the band gaps of LLZO had large undulations at the grain boundaries. The narrow band gaps at the grain boundaries provided electrons more readily during the cycling of batteries, allowing lithium ions to be reduced to lithium metal (Fig. 8a).[187] Hausen *et al.* studied the interface between ceramic particles and the polymer matrix with a high spatial resolution employing electrochemical strain microscopy (ESM). They analyzed the different signals of different materials in terms of friction, contact resonance frequencies, and amplitude signals in terms of lithium-ion accumulation and conduction region (Fig. 8b). They clarified the significant contribution of ceramic-polymer interaction on the conductivity of CPEs.[188]

In addition to the above-mentioned new techniques, there are some new applications of traditional technologies in the research of SSLMBs. For example, Zhang *et al.* used the distribution of relaxation time (DRT) method to couple the EIS impedance spectrum. The characteristic dynamic process presented obvious peaks in the distribution of relaxation time map, and each time constant represented different dynamic processes present in the impedance, achieving direct analysis of the impedance spectrum.[189] Overall, the combination of innovative traditional characterization methods and new detection techniques allows us to gain a deeper understanding of the interfacial characteristics and reaction mechanisms of SSLMBs.

5.2 Model prediction

Chemical and electrochemical reactivity may cause various elements to appear at the interface between the electrolyte and the electrode, resulting in varying degrees of confusion. Various interface models have been developed based on different assumptions about the degree of confusion at the interface.[113,190,191] For example, Wood *et al.* created an efficient and general mesoscopic computational method capable of predicting effective ionic conductivity based on a microstructure of complex polycrystalline oxide-based SSE. They successfully captured the impact of heterogeneity on effective ion conductivity at the atomic and microstructural scales. For the given polycrystalline LLZO microstructure, they established a model to calculate the effective ion diffusion rate in the structure and converted it into ion conductivity, thus achieving the prediction of the electrical properties of LLZO electrolytes

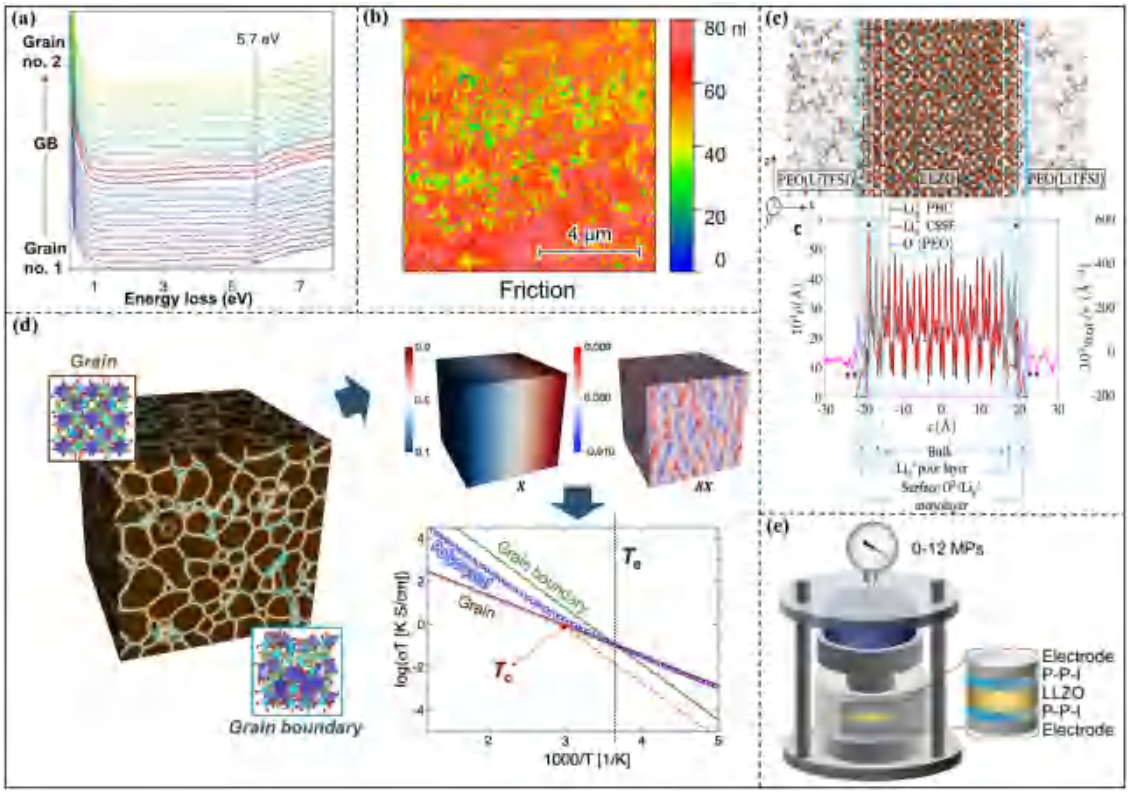

Fig. 8 Research models and practical devices of LLZO-based SSLMBs. (a) Line-scan EELS analysis across GB. Spectra that involve GB contributions are highlighted in red. Reproduced with permission from ref. 187. Copyright 2021 Springer Nature. (b) Friction image of a PEO–LiTFSI with 50 wt.% LLZO. Reproduced with permission from ref. 188. Copyright 2022 Multidisciplinary Digital Publishing Institute. (c) Simulation box for the LLZO/PEO (LiTFSI) system. The LLZO electrolyte is cleaved to the center of the simulation box, creating two interfaces perpendicular to the *x*-axis. Axial density distribution $\rho(x)$ in the equilibrated CSSE (solid red line), in stand-alone LLZO under PBC (dotted black line), and for the O atoms in the PEO polymer chains (solid magenta line) in the equilibrated CSSE. Reproduced with permission from ref. 192. Copyright 2021 American Chemical Society. (d) Example digital representation of a polycrystalline LLZO microstructure, incorporating crystalline grains and atomically disordered grain boundaries. Steady-state profile of Li composition along with its perturbation part within the example microstructure. The curve of ionic conductivity against temperature. Reproduced with permission from ref. 191. Copyright 2021 Springer Nature. (e) Schematic of pressure measurement and the configuration of the P–P–I modified SSLMBs. Reproduced with permission from ref. 206. Copyright 2023 Wiley-VCH.

with different structures (Fig. 8c).[192] Kim *et al.* built an interface modeling based on energy band theory, which enabled efficient interface analysis through customized energy band alignment, and this method was perfectly suited to the introduction of LLZO interfacial analysis.[193] Akhmatskaya *et al.* proposed a model simulating interfacial lithium-ion distribution and revealing the long-term effects of LLZO surfaces on lithium-ion diffusivity. This model could explain the phenomenon of decreasing conductivity at critical packing fractions well below the theoretical permeation threshold (Fig. 8d).[191] Machine-learning interatomic potential has also been developed to accurately predict structural and vibrational properties of LLZO, elasticity, capture effects of grain boundary, *etc.*[194] These models established by capturing phenomena and extracting feature values could provide more inspiration for the interface optimization of LLZO-based batteries.

6. Engineering design

From the perspective of engineering applications, the performance of LLZO-based SSLMBs is comprehensively influenced by factors of different levels, among which interfacial characteristics are the key influencing factor. In engineering, interface problems are usually solved from two aspects: material optimization and stress control.

6.1 Material optimization

From the perspective of material selection, Guo *et al.* compared the thickness, area-specific resistance, and energy density of the LiPON, LLZO sheet, and LLZO-based CPE, respectively. They concluded that LLZO sheet–based SSLMBs are suitable for portable electronics, while LLZO-based CPE-assembled SSLMBs are suitable for electric vehicles.[195,196]

For the interface between cathodes and LLZO, high-potential cathodes may lead to the oxidative decomposition of LLZO. The interaction between lattice oxygen in the fully charged cathode and active substances produced by electrolyte decomposition can generate a large amount of Joule heat, which may lead to catastrophic thermal runaway.[197] Compared with $LiMn_2O_4$ and $LiFeO_4$, $LiCoO_2$ is relatively stable against LLZO electrolytes (see section 3.2). However, Doughty *et al.* found that although it delivered good capacity, $LiCoO_2$

exhibited poor thermal stability than $Li_{1.1}(Ni_{1/3}Co_{1/3}Mn_{1/3})_{0.9}O_2$, $LiMn_2O_4$, and $LiFePO_4$ at high temperatures.[198] In order to assure the electrochemical stability and compatible safety of LLZO against the cathode, further research needs to be done.

6.2 Stress control

The stress change caused by electrode expansion and contraction during the battery cycle is a significant characteristic of LLZO-based SSLMBs. Applying an appropriate amount of external pressure to counteract the stress accumulation might assure the steady operation of the LLZO-based SSLMBs during cycling because stress variations have a noticeable impact on several interfaces of LLZO-based SSLMBs.[199,200] However, applying external stress also has limitations. On the one hand, excessive external pressure can cause the creep of lithium metal, which may force the lithium metal to pass through the voids of LLZO and contact with the cathode.[201] On the other hand, external pressure makes it impossible for the electrode volume to expand in a limited space, which can cause local microstructure changes inside the battery, affecting the electrode interface contact.[202] Researchers have proposed numerous strategies for the rational distribution or compatibility with external pressure. Gallagher *et al.* introduced a thin gold interlayer of 300 nm between the lithium metal and LLZO. In addition, the application of an external pressure of 0.7 MPa significantly improved the cycle performance.[59] The authors found that applying appropriate external pressure can help reduce void formation and suppress the decline of discharge capacity. Li *et al.* found that applying a high stacking pressure of 70 MPa induces creep or plastic deformation of lithium metal at the interface, enhancing interface contact and inhibiting dendrite growth. The effects of the interface design and the pressure are mutual. Therefore, Li *et al.* further constructed an interlayer containing Mo and Li_2S to optimize the interface. The high-hardness metal Mo nanocrystals within the interlayer effectively restrained the growth of lithium dendrites. Simultaneously, the electrically insulating Li_2S significantly enhanced interface wettability, impeding the deep penetration of lithium dendrites into LLZO. Under the mutual influence of external pressure and the interlayers, SSLMBs have gained a significantly extended life.[203] It is evident that various strategies can be paired with the optimized external pressure to achieve a comprehensive optimization of performance.

From an engineering perspective, for a single cell that requires external molds for preload, relative tests need to be considered at the pack level. Moreover, stacking pressure from several megapascals to tens of megapascals is required for pack assembly, which is difficult to achieve in practical applications.[199,204] The materials used to buffer stress are also constantly being improved. For example, the super-elasticity of shape memory alloy based on stress-induced martensite transformation could fully absorb the considerable volume expansion strain of the electrode. During the recovery process of the electrode, the stress of the shape memory alloy is released.[205] Notably, due to the need of external pressurization devices for pressure control, the energy density of LLZO-based SSLMB can be reduced. Besides, although laboratory-level pressurization devices can simulate the response characteristics of SSLMBs under different pressure conditions, there are still transferable difficulties in applying the explored laws to engineering practice.

Reducing stacking pressure may be a more practical direction for commercialization. A phase-changeable interlayer was developed to achieve self-adhesive and dynamic conformal electrode/LLZO contact. The strong adhesive strengths of the phase-changeable interlayer enable SSLMBs to resist up to 250 N pulling force, endowing SSLMBs with ideal interfacial integrity without extra stack pressure (Fig. 8e).[206] Sakamoto *et al.* designed a composite lithium anode containing lithium metal and carbon nanotubes (CNTs). This composite anode enhanced the effective diffusion of Li^+ because CNTs promoted the transport of Li^+ at the anode/LLZO interface. Without applying external stack pressure, the SSLMB prepared with this composite lithium anode achieved a discharge capacity of over 20 mA h cm^{-2} at 100 mA cm^{-2}.[207]

Summary and perspectives

Due to its high ion conductivity, large electrochemical window, high shear modulus, and strong chemical stability against lithium metal, the LLZO-based SSEs are one of the most promising materials for SSLMBs. Although the LLZO-based SSLMBs have been developed for decades, there are still issues with the anode/electrolyte interface, cathode/electrolyte interface, and internal interfaces of the LLZO-based SSEs. In this review, we carried out an extensive investigation of the above-mentioned crucial interfaces and outlined the relevant techniques for interface optimization. On this basis, some perspectives are proposed as follows:

(1) For the interface of the anode/electrolyte, the growth of the hydrophobic Li_2CO_3 layer on the LLZO surface is an important inducement for the impedance increase of the battery. While the high electronic conductivity and uneven local current caused by the microstructure defects could promote the growth of lithium dendrites. Therefore, designing precise and efficient integrated methods to remove the Li_2CO_3 passivation layer while constructing a stable intermediate transition layer of ion/electron conductors is an important direction for optimizing the interface of anodes/electrolytes.

(2) For the interface of cathodes/electrolytes, it is necessary to pay attention to the efficient combination of process methods and material screening. Both the co-sintering and surface coating technologies could effectively alleviate the interfacial contact problem. The transition layer of the soft ion conductor is expected to maintain interface stability with the dynamic volume expansion of the electrode during the battery cycling process. Meanwhile, the stability of the material itself and the high compatibility of the intermediate layer are the key points that need to be emphasized in the process of optimizing the interface. The development of advanced calculation methods will provide ideas for efficiently selecting suitable interphase materials.

(3) For the internal interfaces of the SSEs, the barrier of mass transfer caused by the highly active interface of LLZO sheets can be optimized using methods such as electrolyte densification, grain boundary regulation, and material purification. CPEs that balance the advantages of LLZO and polymers are an important development direction in the future, but the problems of non-uniform mass transfer and the heterogeneous stability they face will be highlighted during long cycles. Therefore, it is necessary to design the composition, morphology, and structure of the CPEs to balance the stability of interphase interactions and ion conductivity. Interface modeling combined with ion transport paths and energy variation characteristics will be the key strategies to seek a better balance.

(4) From an engineering perspective, the real-world application of SSLMBs still remains a huge challenge. A deep understanding and comprehensive consideration of various interface issues are crucial for achieving high-performance LLZO-based SSLMBs. In the future, the stability of the internal interface of the battery could be improved by the dynamic balance changes of the electrodes and electrolytes with more elastic buffer capacity. In addition, the advanced design of the system structure will play a positive role in the application of the batteries. Thus, besides the development of the components and structures inside the ''internal interface'' between the electrode and the electrolyte at the level of the battery, it is crucial to coordinate and optimize the ''external interface'' between the battery and structural components at the pack level.

Conflicts of interest

There are no conflicts to declare.

Acknowledgements

This work was financially supported by the National Key R&D Program of China (2020YFE0204500), National Natural Science Foundation of China (52171194, 52071311, 52271140, U22A20437), CAS Project for Young Scientists in Basic Research (YSBR-058), Changchun Science and Technology Development Plan Funding Project (21ZY06), Youth Innovation Promotion Association CAS (2020230), Natural Science Foundation of China Excellent Young Scientists (Overseas), and the China Postdoctoral Science Foundation (2022M713070).

References

1 W. Wang and P. N. Kumta, Nanostructured Hybrid Silicon/Carbon Nanotube Heterostructures: Reversible High-Capacity Lithium-Ion Anodes, *ACS Nano*, 2010, **4**, 2233–2241.
2 W. L. An, P. He, Z. Z. Che, C. M. Xiao, E. M. Guo, C. L. Pang, X. Q. He, J. G. Ren, G. H. Yuan, N. Du, D. R. Yang, D. L. Peng and Q. B. Zhang, Scalable Synthesis of Pore-Rich Si/C@C Core-Shell-Structured Microspheres for Practical Long-Life Lithium-Ion Battery Anodes, *ACS Appl. Mater. Interfaces*, 2022, **14**, 10308–10318.
3 Y. M. Sun, N. A. Liu and Y. Cui, Promises and challenges of nanomaterials for lithium-based rechargeable batteries, *Nat. Energy*, 2016, **1**, 16071.
4 X. B. Cheng and Q. Zhang, Dendrite-free lithium metal anodes: stable solid electrolyte interphases for high-efficiency batteries, *J. Mater. Chem. A*, 2015, **3**, 7207–7209.
5 W. Xu, J. L. Wang, F. Ding, X. L. Chen, E. Nasybutin, Y. H. Zhang and J. G. Zhang, Lithium metal anodes for rechargeable batteries, *Energy Environ. Sci.*, 2014, **7**, 513–537.
6 J. Langdon and A. Manthiram, Crossover Effects in Batteries with High-Nickel Cathodes and Lithium-Metal Anodes, *Adv. Funct. Mater.*, 2021, **31**, 2010267.
7 Q.-K. Zhang, X.-Q. Zhang, J. Wan, N. Yao, T.-L. Song, J. Xie, L.-P. Hou, M.-Y. Zhou, X. Chen, B.-Q. Li, R. Wen, H.-J. Peng, Q. Zhang and J.-Q. Huang, Homogeneous and mechanically stable solid-electrolyte interphase enabled by trioxane-modulated electrolytes for lithium metal batteries, *Nat. Energy*, 2023, **8**, 725–735.
8 B. Liu, J.-G. Zhang and W. Xu, Advancing Lithium Metal Batteries, *Joule*, 2018, **2**, 833–845.
9 W. Xu, J. Wang, F. Ding, X. Chen, E. Nasybulin, Y. Zhang and J.-G. Zhang, Lithium metal anodes for rechargeable batteries, *Energy Environ. Sci.*, 2014, **7**, 513–537.
10 L. Q. Xu, J. Y. Li, W. T. Deng, H. L. Shuai, S. Li, Z. F. Xu, J. H. Li, H. S. Hou, H. J. Peng, G. Q. Zou and X. B. Ji, Garnet Solid Electrolyte for Advanced All-Solid-State Li Batteries, *Adv. Energy Mater.*, 2021, **11**, 2000648.
11 C. H. Wang, J. T. Kim, C. S. Wang and X. L. Sun, Progress and Prospects of Inorganic Solid-State Electrolyte-Based All-Solid-State Pouch Cells, *Adv. Mater.*, 2023, **35**, 2209074.
12 Z. Li, J. L. Fu, X. Y. Zhou, S. W. Gui, L. Wei, H. Yang, H. Li and X. Guo, Ionic Conduction in Polymer-Based Solid Electrolytes, *Adv. Sci.*, 2023, **10**, 2201718.
13 J. H. Wu, S. F. Liu, F. D. Han, X. Y. Yao and C. S. Wang, Lithium/Sulfide All-Solid-State Batteries using Sulfide Electrolytes, *Adv. Mater.*, 2021, **33**, 2000751.
14 Q. Zhao, S. Stalin, C.-Z. Zhao and L. A. Archer, Designing solid-state electrolytes for safe, energy-dense batteries, *Nat. Rev. Mater.*, 2020, **5**, 229–252.
15 F. D. Han, Y. Z. Zhu, X. F. He, Y. F. Mo and C. S. Wang, Electrochemical Stability of $Li_{10}GeP_2S_{12}$ and $Li_7La_3Zr_2O_{12}$ Solid Electrolytes, *Adv. Energy Mater.*, 2016, **6**, 1501590.
16 C. Wang, K. Fu, S. P. Kammampata, D. W. McOwen, A. J. Samson, L. Zhang, G. T. Hitz, A. M. Nolan, E. D. Wachsman, Y. Mo, V. Thangadurai and L. Hu, Garnet-Type Solid-State Electrolytes: Materials, Interfaces, and Batteries, *Chem. Rev.*, 2020, **120**, 4257–4300.
17 V. Thangadurai, D. Pinzaru, S. Narayanan and A. K. Baral, Fast Solid-State Li Ion Conducting Garnet-Type Structure Metal Oxides for Energy Storage, *J. Phys. Chem. Lett.*, 2015, **6**, 292–299.
18 S. Yu, R. D. Schmidt, R. Garcia-Mendez, E. Herbert, N. J. Dudney, J. B. Wolfenstine, J. Sakamoto and D. J. Siegel,

Elastic Properties of the Solid Electrolyte $Li_7La_3Zr_2O_{12}$ (LLZO), *Chem. Mat.*, 2016, **28**, 197–206.

19 A. J. Samson, K. Hofstetter, S. Bag and V. Thangadurai, A bird's-eye view of Li-stuffed garnet-type $Li_7La_3Zr_2O_{12}$ ceramic electrolytes for advanced all-solid-state Li batteries, *Energy Environ. Sci.*, 2019, **12**, 2957–2975.

20 R. Murugan, V. Thangadurai and W. Weppner, Fast lithium ion conduction in garnet-type $Li_7La_3Zr_2O_{12}$, *Angew. Chem., Int. Ed.*, 2007, **46**, 7778–7781.

21 V. Thangadurai, S. Narayanan and D. Pinzaru, Garnet-type solid-state fast Li ion conductors for Li batteries: critical review, *Chem. Soc. Rev.*, 2014, **43**, 4714–4727.

22 S. Kim, G. Yoon, S.-K. Jung, S. Park, J.-S. Kim, K. Yoon, S. Lee and K. Kang, High-Power Hybrid Solid-State Lithium-Metal Batteries Enabled by Preferred Directional Lithium Growth Mechanism, *ACS Energy Lett.*, 2023, **8**, 9–20.

23 L. Cheng, E. J. Crumlin, W. Chen, R. M. Qiao, H. M. Hou, S. F. Lux, V. Zorba, R. Russo, R. Kostecki, Z. Liu, K. Persson, W. L. Yang, J. Cabana, T. Richardson, G. Y. Chen and M. Doeff, The origin of high electrolyte-electrode interfacial resistances in lithium cells containing garnet type solid electrolytes, *Phys. Chem. Chem. Phys.*, 2014, **16**, 18294–18300.

24 T. Liu, Y. Y. Ren, Y. Shen, S. X. Zhao, Y. H. Lin and C. W. Nan, Achieving high capacity in bulk-type solid-state lithium ion battery based on $Li_{6.75}La_3Zr_{1.75}Ta_{0.25}O_{12}$ electrolyte: Interfacial resistance, *J. Power Sources*, 2016, **324**, 349–357.

25 Y. H. Xiao, Y. Wang, S. H. Bo, J. C. Kim, L. J. Miara and G. Ceder, Understanding interface stability in solid-state batteries, *Nat. Rev. Mater.*, 2020, **5**, 105–126.

26 J.-F. Wu, E.-Y. Chen, Y. Yu, L. Liu, Y. Wu, W. K. Pang, V. K. Peterson and X. Guo, Gallium-Doped $Li_7La_3Zr_2O_{12}$ Garnet-Type Electrolytes with High Lithium-Ion Conductivity, *ACS Appl. Mater. Interfaces*, 2017, **9**, 1542–1552.

27 S. Xia, X. Wu, Z. Zhang, Y. Cui and W. Liu, Practical Challenges and Future Perspectives of All-Solid-State Lithium-Metal Batteries, *Chem*, 2019, **5**, 753–785.

28 J.-F. Wu, B.-W. Pu, D. Wang, S.-Q. Shi, N. Zhao, X. Guo and X. Guo, In Situ Formed Shields Enabling Li_2CO_3-Free Solid Electrolytes: A New Route to Uncover the Intrinsic Lithiophilicity of Garnet Electrolytes for Dendrite-Free Li-Metal Batteries, *ACS Appl. Mater. Interfaces*, 2019, **11**, 898–905.

29 S. Chen, Z. Nie, F. Tian, L. Nie, R. Wei, J. Yu, T. Gao, Z. Sun, N. Yang and W. Liu, The Influence of Surface Chemistry on Critical Current Density for Garnet Electrolyte, *Adv. Funct. Mater.*, 2022, **32**, 2113318.

30 A. Sharafi, S. Yu, M. Naguib, M. Lee, C. Ma, H. M. Meyer, J. Nanda, M. Chi, D. J. Siegel and J. Sakamoto, Impact of air exposure and surface chemistry on Li-$Li_7La_3Zr_2O_{12}$ interfacial resistance, *J. Mater. Chem. A*, 2017, **5**, 13475–13487.

31 C. Ma, E. Rangasamy, C. Liang, J. Sakamoto, K. L. More and M. Chi, Excellent stability of a lithium-ion-conducting solid electrolyte upon reversible Li^+/H^+ exchange in aqueous solutions, *Angew. Chem., Int. Ed.*, 2015, **54**, 129–133.

32 B. Chen, J. Zhang, T. Zhang, R. Wang, J. Zheng, Y. Zhai and X. Liu, Constructing a Superlithiophilic 3D Burr-Microsphere Interface on Garnet for High-Rate and Ultra-Stable Solid-State Li Batteries, *Adv. Sci.*, 2023, **10**, 2207056.

33 M. Siniscalchi, J. Liu, J. S. Gibson, S. J. Turrell, J. Aspinall, R. S. Weatherup, M. Pasta, S. C. Speller and C. R. M. Grovenor, On the Relative Importance of Li Bulk Diffusivity and Interface Morphology in Determining the Stripped Capacity of Metallic Anodes in Solid-State Batteries, *ACS Energy Lett.*, 2022, **7**, 3593–3599.

34 Q. Chen and K. Sieradzki, Spontaneous evolution of bicontinuous nanostructures in dealloyed Li-based systems, *Nat. Mater.*, 2013, **12**, 1102–1106.

35 S. Yu, R. D. Schmidt, R. Garcia-Mendez, E. Herbert, N. J. Dudney, J. B. Wolfenstine, J. Sakamoto and D. J. Siegel, Elastic Properties of the Solid Electrolyte $Li_7La_3Zr_2O_{12}$ (LLZO), *Chem. Mat.*, 2015, **28**, 197–206.

36 X. Ji, S. Hou, P. Wang, X. He, N. Piao, J. Chen, X. Fan and C. Wang, Solid-State Electrolyte Design for Lithium Dendrite Suppression, *Adv. Mater.*, 2020, **32**, 2002741.

37 X. Fan, X. Ji, F. Han, J. Yue, J. Chen, L. Chen, T. Deng, J. Jiang and C. Wang, Fluorinated solid electrolyte interphase enables highly reversible solid-state Li metal battery, *Sci. Adv.*, 2018, **4**, eaau9245.

38 T. Krauskopf, B. Mogwitz, H. Hartmann, D. K. Singh, W. G. Zeier and J. Janek, The Fast Charge Transfer Kinetics of the Lithium Metal Anode on the Garnet-Type Solid Electrolyte $Li_{6.25}Al_{0.25}La_3Zr_2O_{12}$, *Adv. Energy Mater.*, 2020, **10**, 2000945.

39 W. Manalastas, J. Rikarte, R. J. Chater, R. Brugge, A. Aguadero, L. Buannic, A. Llordés, F. Aguesse and J. Kilner, Mechanical failure of garnet electrolytes during Li electrodeposition observed by in-operando microscopy, *J. Power Sources*, 2019, **412**, 287–293.

40 S. Yu and D. J. Siegel, Grain Boundary Softening: A Potential Mechanism for Lithium Metal Penetration through Stiff Solid Electrolytes, *ACS Appl. Mater. Interfaces*, 2018, **10**, 38151–38158.

41 E. J. Cheng, A. Sharafi and J. Sakamoto, Intergranular Li metal propagation through polycrystalline $Li_{6.25}Al_{0.25}La_3Zr_2O_{12}$ ceramic electrolyte, *Electrochim. Acta*, 2017, **223**, 85–91.

42 X. Liu, R. Garcia-Mendez, A. R. Lupini, Y. Cheng, Z. D. Hood, F. Han, A. Sharafi, J. C. Idrobo, N. J. Dudney, C. Wang, C. Ma, J. Sakamoto and M. Chi, Local electronic structure variation resulting in Li 'filament' formation within solid electrolytes, *Nat. Mater.*, 2021, **20**, 1485–1491.

43 H.-K. Tian, Z. Liu, Y. Ji, L.-Q. Chen and Y. Qi, Interfacial Electronic Properties Dictate Li Dendrite Growth in Solid Electrolytes, *Chem. Mat.*, 2019, **31**, 7351–7359.

44 F. Han, A. S. Westover, J. Yue, X. Fan, F. Wang, M. Chi, D. N. Leonard, N. Dudney, H. Wang and C. Wang, High electronic conductivity as the origin of lithium dendrite formation within solid electrolytes, *Nat. Energy*, 2019, **4**, 187–196.

45 F. Aguesse, W. Manalastas, L. Buannic, J. M. Lopez del Amo, G. Singh, A. Llordes and J. Kilner, Investigating the Dendritic Growth during Full Cell Cycling of Garnet Electrolyte in Direct Contact with Li Metal, *ACS Appl. Mater. Interfaces*, 2017, **9**, 3808–3816.

46 H. Zheng, G. Li, R. Ouyang, Y. Han, H. Zhu, Y. Wu, X. Huang, H. Liu and H. Duan, Origin of Lithiophilicity of Lithium Garnets: Compositing or Cleaning?, *Adv. Funct. Mater.*, 2022, **32**, 2205778.

47 Z. Qin, Y. Xie, X. Meng, D. Qian, C. Shan, D. Mao, G. He, Z. Zheng, L. Wan and Y. Huang, Interface engineering for garnet-type electrolyte enables low interfacial resistance in solid-state lithium batteries, *Chem. Eng. J.*, 2022, **447**, 137538.

48 S. Vema, F. N. Sayed, S. Nagendran, B. Karagoz, C. Sternemann, M. Paulus, G. Held and C. P. Grey, Understanding the Surface Regeneration and Reactivity of Garnet Solid-State Electrolytes, *ACS Energy Lett.*, 2023, **8**, 3476–3484.

49 H. Huo, Y. Chen, N. Zhao, X. Lin, J. Luo, X. Yang, Y. Liu, X. Guo and X. Sun, In-situ formed Li_2CO_3-free garnet/Li interface by rapid acid treatment for dendrite-free solid-state batteries, *Nano Energy*, 2019, **61**, 119–125.

50 Y. Ruan, Y. Lu, X. Huang, J. Su, C. Sun, J. Jin and Z. Wen, Acid induced conversion towards a robust and lithiophilic interface for Li-$Li_7La_3Zr2O_{12}$ solid-state batteries, *J. Mater. Chem. A*, 2019, **7**, 14565–14574.

51 Y. Ruan, Y. Lu, Y. Li, C. Zheng, J. Su, J. Jin, T. Xiu, Z. Song, M. E. Badding and Z. Wen, A 3D Cross-Linking Lithiophilic and Electronically Insulating Interfacial Engineering for Garnet-Type Solid-State Lithium Batteries, *Adv. Funct. Mater.*, 2021, **31**, 2007815.

52 C. Guo, Y. Shen, P. Mao, K. Liao, M. Du, R. Ran, W. Zhou and Z. Shao, Grafting of Lithiophilic and Electron-Blocking Interlayer for Garnet-Based Solid-State Li Metal Batteries via One-Step Anhydrous Poly-Phosphoric Acid Post-Treatment, *Adv. Funct. Mater.*, 2023, **33**, 2213443.

53 H. Duan, W. P. Chen, M. Fan, W. P. Wang, L. Yu, S. J. Tan, X. Chen, Q. Zhang, S. Xin, L. J. Wan and Y. G. Guo, Building an Air Stable and Lithium Deposition Regulable Garnet Interface from Moderate-Temperature Conversion Chemistry, *Angew. Chem., Int. Ed.*, 2020, **59**, 12069–12075.

54 X. Yang, S. Tang, C. Zheng, F. Ren, Y. Huang, X. Fei, W. Yang, S. Pan, Z. Gong and Y. Yang, From Contaminated to Highly Lithiated Interfaces: A Versatile Modification Strategy for Garnet Solid Electrolytes, *Adv. Funct. Mater.*, 2023, **33**, 2209120.

55 T. Krauskopf, B. Mogwitz, C. Rosenbach, W. G. Zeier and J. Janek, Diffusion Limitation of Lithium Metal and Li-Mg Alloy Anodes on LLZO Type Solid Electrolytes as a Function of Temperature and Pressure, *Adv. Energy Mater.*, 2019, **9**, 1902568.

56 Y. Jiang, Y. Li, P. Zhou, Z. Lan, Y. Lu, C. Wu and M. Yan, Ultrafast, Highly Reversible, and Cycle-Stable Lithium Storage Boosted by Pseudocapacitance in Sn-Based Alloying Anodes, *Adv. Mater.*, 2017, **29**, 1606499.

57 X. Xiang, S. Cao, F. Chen, Q. Shen and L. Zhang, Communication-Li/$Li_7La_3Zr_2O_{12}$ Interfacial Modification by Constructing a Layer of Cu-Li Alloy, *J. Electrochem. Soc.*, 2019, **166**, A3028–A3030.

58 R. Dubey, J. Sastre, C. Cancellieri, F. Okur, A. Förster, L. Pompizii, A. Priebe, Y. E. Romanyuk, L. P. H. Jeurgens, M. V. Kovalenko and K. V. Kravchyk, Building a Better Li-Garnet Solid Electrolyte/Metallic Li Interface with Antimony, *Adv. Energy Mater.*, 2021, **11**, 2102086.

59 A. C. Thenuwara, E. L. Thompson, T. F. Malkowski, K. D. Parrotte, K. E. Lostracco, S. Narayan, R. T. Rooney, L. A. Seeley, M. R. Borges, B. D. Conway, Z. Song, M. E. Badding and K. G. Gallagher, Interplay among Metallic Interlayers, Discharge Rate, and Pressure in LLZO-Based Lithium-Metal Batteries, *ACS Energy Lett.*, 2023, **8**, 4016–4023.

60 X. He, X. Ji, B. Zhang, N. D. Rodrigo, S. Hou, K. Gaskell, T. Deng, H. Wan, S. Liu, J. Xu, B. Nan, B. L. Lucht and C. Wang, Tuning Interface Lithiophobicity for Lithium Metal Solid-State Batteries, *ACS Energy Lett.*, 2022, **7**, 131–139.

61 Z. Wan, K. Shi, Y. Huang, L. Yang, Q. Yun, L. Chen, F. Ren, F. Kang and Y.-B. He, Three-dimensional alloy interface between $Li_{6.4}La_3Zr_{1.4}Ta_{0.6}O_{12}$ and Li metal to achieve excellent cycling stability of all-solid-state battery, *J. Power Sources*, 2021, **505**, 230062.

62 W. Feng, X. Dong, Z. Lai, X. Zhang, Y. Wang, C. Wang, J. Luo and Y. Xia, Building an Interfacial Framework: Li/Garnet Interface Stabilization through a Cu_6Sn_5 Layer, *ACS Energy Lett.*, 2019, **4**, 1725–1731.

63 Y. You, F. Zheng, D. Zhang, C. Zhao, C. Hu, X. Cao, Z.-Z. Zhu and S. Wu, Effect of Charge Non-Uniformity on the Lithium Dendrites and Improvement by the LiF Interfacial Layer, *ACS Appl. Energy Mater.*, 2022, **5**, 15078–15085.

64 Y. Niu, Z. Yu, Y. Zhou, J. Tang, M. Li, Z. Zhuang, Y. Yang, X. Huang and B. Tian, Constructing stable Li-solid electrolyte interphase to achieve dendrites-free solid-state battery: A nano-interlayer/Li pre-reduction strategy, *Nano Res.*, 2022, **15**, 7180–7189.

65 T. Deng, X. Ji, Y. Zhao, L. Cao, S. Li, S. Hwang, C. Luo, P. Wang, H. Jia, X. Fan, X. Lu, D. Su, X. Sun, C. Wang and J. G. Zhang, Tuning the Anode-Electrolyte Interface Chemistry for Garnet-Based Solid-State Li Metal Batteries, *Adv. Mater.*, 2020, **32**, 2000030.

66 H. Huo, Y. Chen, R. Li, N. Zhao, J. Luo, J. G. Pereira da Silva, R. Mücke, P. Kaghazchi, X. Guo and X. Sun, Design of a mixed conductive garnet/Li interface for dendrite-free solid lithium metal batteries, *Energy Environ. Sci.*, 2020, **13**, 127–134.

67 J. Jiang, Y. Ou, S. Lu, C. Shen, B. Li, X. Liu, Y. Jiang, B. Zhao and J. Zhang, In-situ construction of Li-Mg/LiF conductive layer to achieve an intimate lithium-garnet interface for all-solid-state Li metal battery, *Energy Storage Mater.*, 2022, **50**, 810–818.

68 X. Han, Y. Gong, K. K. Fu, X. He, G. T. Hitz, J. Dai, A. Pearse, B. Liu, H. Wang, G. Rubloff, Y. Mo, V. Thangadurai,

E. D. Wachsman and L. Hu, Negating interfacial impedance in garnet-based solid-state Li metal batteries, *Nat. Mater.*, 2017, **16**, 572–579.

69 S. Guo, Y. Li, B. Li, N. S. Grundish, A. M. Cao, Y. G. Sun, Y. S. Xu, Y. Ji, Y. Qiao, Q. Zhang, F. Q. Meng, Z. H. Zhao, D. Wang, X. Zhang, L. Gu, X. Yu and L. J. Wan, Coordination-Assisted Precise Construction of Metal Oxide Nanofilms for High-Performance Solid-State Batteries, *J. Am. Chem. Soc.*, 2022, **144**, 2179–2188.

70 L. Zhang, J. Yang, K. Jing, C. Li, Y. Gao, X. Wang and Q. Fang, Thickness-Dependent Beneficial Effect of the ZnO Layer on Tailoring the Li/$Li_7La_3Zr_2O_{12}$ Interface, *ACS Appl. Mater. Interfaces*, 2020, **12**, 13836–13841.

71 Y. Wei, H. Xu, H. Cheng, W. Guan, J. Yang, Z. Li and Y. Huang, An oxygen vacancy-rich ZnO layer on garnet electrolyte enables dendrite-free solid state lithium metal batteries, *Chem. Eng. J.*, 2022, **433**, 133665.

72 S. Guo, T.-T. Wu, Y.-G. Sun, S.-D. Zhang, B. Li, H.-S. Zhang, M.-Y. Qi, X.-H. Liu, A.-M. Cao and L.-J. Wan, Interface Engineering of a Ceramic Electrolyte by Ta_2O_5 Nanofilms for Ultrastable Lithium Metal Batteries, *Adv. Funct. Mater.*, 2022, **32**, 2201498.

73 F. Zhu, W. Deng, B. Zhang, H. Wang, L. Xu, H. Liu, Z. Luo, G. Zou, H. Hou and X. Ji, In-situ construction of multifunctional interlayer enabled dendrite-free garnet-based solid-state batteries, *Nano Energy*, 2023, **111**, 108416.

74 B. Zhao, W. Ma, B. Li, X. Hu, S. Lu, X. Liu, Y. Jiang and J. Zhang, A fast and low-cost interface modification method to achieve high-performance garnet-based solid-state lithium metal batteries, *Nano Energy*, 2022, **91**, 106643.

75 L. Zhai, K. Yang, F. Jiang, W. Liu, Z. Yan and J. Sun, High-performance solid-state lithium metal batteries achieved by interface modification, *J. Energy Chem.*, 2023, **79**, 357–364.

76 S. Lee, K. S. Lee, S. Kim, K. Yoon, S. Han, M. H. Lee, Y. Ko, J. H. Noh, W. Kim and K. Kang, Design of a lithiophilic and electron-blocking interlayer for dendrite-free lithium-metal solid-state batteries, *Sci. Adv.*, 2022, **8**, eabq0153.

77 B. Q. Xiong, S. Chen, X. Luo, Q. Nian, X. Zhan, C. Wang and X. Ren, Plastic Monolithic Mixed-Conducting Interlayer for Dendrite-Free Solid-State Batteries, *Adv. Sci.*, 2022, **9**, 2105924.

78 H. Huo, J. Gao, N. Zhao, D. Zhang, N. G. Holmes, X. Li, Y. Sun, J. Fu, R. Li, X. Guo and X. Sun, A flexible electron-blocking interfacial shield for dendrite-free solid lithium metal batteries, *Nat. Commun.*, 2021, **12**, 176.

79 W. Feng, J. Hu, G. Qian, Z. Xu, G. Zan, Y. Liu, F. Wang, C. Wang and Y. Xia, Stabilization of garnet/Li interphase by diluting the electronic conductor, *Sci. Adv.*, 2022, **8**, eadd8972.

80 T. Wang, J. Duan, B. Zhang, W. Luo, X. Ji, H. Xu, Y. Huang, L. Huang, Z. Song, J. Wen, C. Wang, Y. Huang and J. B. Goodenough, A self-regulated gradient interphase for dendrite-free solid-state Li batteries, *Energy Environ. Sci.*, 2022, **15**, 1325–1333.

81 Z. Bi, W. Huang, S. Mu, W. Sun, N. Zhao and X. Guo, Dual-interface reinforced flexible solid garnet batteries enabled by in-situ solidified gel polymer electrolytes, *Nano Energy*, 2021, **90**, 106498.

82 H. Zhang, F. Okur, C. Cancellieri, L. P. H. Jeurgens, A. Parrilli, D. T. Karabay, M. Nesvadba, S. Hwang, A. Neels, M. V. Kovalenko and K. V. Kravchyk, Bilayer Dense-Porous $Li_7La_3Zr_2O_{12}$ Membranes for High-Performance Li-Garnet Solid-State Batteries, *Adv. Sci.*, 2023, **10**, 2205821.

83 R. Xu, F. Liu, Y. Ye, H. Chen, R. R. Yang, Y. Ma, W. Huang, J. Wan and Y. Cui, A Morphologically Stable Li/Electrolyte Interface for All-Solid-State Batteries Enabled by 3D-Micropatterned Garnet, *Adv. Mater.*, 2021, **33**, 2104009.

84 C. Yang, L. Zhang, B. Liu, S. Xu, T. Hamann, D. McOwen, J. Dai, W. Luo, Y. Gong, E. D. Wachsman and L. Hu, Continuous plating/stripping behavior of solid-state lithium metal anode in a 3D ion-conductive framework, *Proc. Natl. Acad. Sci. U. S. A.*, 2018, **115**, 3770–3775.

85 K. Fu, Y. Gong, G. T. Hitz, D. W. McOwen, Y. Li, S. Xu, Y. Wen, L. Zhang, C. Wang, G. Pastel, J. Dai, B. Liu, H. Xie, Y. Yao, E. D. Wachsman and L. Hu, Three-dimensional bilayer garnet solid electrolyte based high energy density lithium metal-sulfur batteries, *Energy Environ. Sci.*, 2017, **10**, 1568–1575.

86 S. Xu, D. W. McOwen, C. Wang, L. Zhang, W. Luo, C. Chen, Y. Li, Y. Gong, J. Dai, Y. Kuang, C. Yang, T. R. Hamann, E. D. Wachsman and L. Hu, Three-Dimensional, Solid-State Mixed Electron-Ion Conductive Framework for Lithium Metal Anode, *Nano Lett.*, 2018, **18**, 3926–3933.

87 K. Lee, S. Han, J. Lee, S. Lee, J. Kim, Y. Ko, S. Kim, K. Yoon, J.-H. Song, J. H. Noh and K. Kang, Multifunctional Interface for High-Rate and Long-Durable Garnet-Type Solid Electrolyte in Lithium Metal Batteries, *ACS Energy Lett.*, 2022, **7**, 381–389.

88 J. C. Stallard, L. Wheatcroft, S. G. Booth, R. Boston, S. A. Corr, M. F. L. De Volder, B. J. Inkson and N. A. Fleck, Mechanical properties of cathode materials for lithium-ion batteries, *Joule*, 2022, **6**, 984–1007.

89 S. Lou, Q. Liu, F. Zhang, Q. Liu, Z. Yu, T. Mu, Y. Zhao, J. Borovilas, Y. Chen, M. Ge, X. Xiao, W.-K. Lee, G. Yin, Y. Yang, X. Sun and J. Wang, Insights into interfacial effect and local lithium-ion transport in polycrystalline cathodes of solid-state batteries, *Nat. Commun.*, 2020, **11**, 5700.

90 N. J. J. de Klerk and M. Wagemaker, Space-Charge Layers in All-Solid-State Batteries; Important or Negligible?, *ACS Appl. Energy Mater.*, 2018, **1**, 5609–5618.

91 C.-Y. Yu, J. Choi, J. Han, E. Lee and J.-H. Kim, Phase Stability of Garnet Solid-Electrolyte Interfacing with Various Cathodes in All Solid-State Batteries, *J. Electrochem. Soc.*, 2022, **169**, 020520.

92 Y. Kim, D. Kim, R. Bliem, G. Vardar, I. Waluyo, A. Hunt, J. T. Wright, J. P. Katsoudas and B. Yildiz, Thermally Driven Interfacial Degradation between $Li_7La_3Zr_2O_{12}$ Electrolyte and $LiNi_{0.6}Mn_{0.2}Co_{0.2}O_2$ Cathode, *Chem. Mat.*, 2020, **32**, 9531–9541.

93 Y. Kim, I. Waluyo, A. Hunt and B. Yildiz, Avoiding CO_2 Improves Thermal Stability at the Interface of $Li_7La_3Zr_2O_{12}$ Electrolyte with Layered Oxide Cathodes, *Adv. Energy Mater.*, 2022, **12**, 2102741.

94 S. Hong, S. H. Song, M. Cho, S. Kim, S. H. Yu, D. Lee and H. Kim, Structural and Chemical Compatibilities of $Li_{1-x}Ni_{0.5}Co_{0.2}Mn_{0.3}O_2$ Cathode Material with Garnet-Type Solid Electrolyte for All-Solid-State Batteries, *Small*, 2021, **17**, 2103306.

95 C. Roitzheim, Y. J. Sohn, L.-Y. Kuo, G. Häuschen, M. Mann, D. Sebold, M. Finsterbusch, P. Kaghazchi, O. Guillon and D. Fattakhova-Rohlfing, All-Solid-State Li Batteries with NCM-Garnet-Based Composite Cathodes: The Impact of NCM Composition on Material Compatibility, *ACS Appl. Energy Mater.*, 2022, **5**, 6913–6926.

96 W. S. Scheld, S. Lobe, C. Dellen, M. Ihrig, G. Häuschen, L. C. Hoff, M. Finsterbusch, S. Uhlenbruck, O. Guillon and D. Fattakhova-Rohlfing, Rapid thermal processing of garnet-based composite cathodes, *J. Power Sources*, 2022, **545**, 231872.

97 G. Zhong, C. Wang, R. Wang, W. Ping, S. Xu, H. Qiao, M. Cui, X. Wang, Y. Zhou, D. J. Kline, M. R. Zachariah and L. Hu, Rapid, high-temperature microwave soldering toward a high-performance cathode/electrolyte interface, *Energy Storage Mater.*, 2020, **30**, 385–391.

98 F. Han, J. Yue, C. Chen, N. Zhao, X. Fan, Z. Ma, T. Gao, F. Wang, X. Guo and C. Wang, Interphase Engineering Enabled All-Ceramic Lithium Battery, *Joule*, 2018, **2**, 497–508.

99 X. Liu, X. Kong, W. Xiang, Y. Jiang, B. Xiong, W. Ping, C. Xia, D. Huan and C. Wang, $LiCoO_2$ sintering aid towards cathode-interface-enhanced garnet electrolytes, *J. Energy Chem.*, 2023, **84**, 181–188.

100 P. Barai, A. T. Ngo, B. Narayanan, K. Higa, L. A. Curtiss and V. Srinivasan, The Role of Local Inhomogeneities on Dendrite Growth in LLZO-Based Solid Electrolytes, *J. Electrochem. Soc.*, 2020, **167**, 100537.

101 A. V. Morozov, H. Paik, A. O. Boev, D. A. Aksyonov, S. A. Lipovskikh, K. J. Stevenson, J. L. M. Rupp and A. M. Abakumov, Thermodynamics as a Driving Factor of $LiCoO_2$ Grain Growth on Nanocrystalline Ta-LLZO Thin Films for All-Solid-State Batteries, *ACS Appl. Mater. Interfaces*, 2022, **14**, 39907–39916.

102 G. H. Kim, M. J. Kim, H. B. Kim, J. H. Ryu and H. C. Lee, Preparation and Characterization of Sol-Gel-Driven $Li_xLa_3Zr_2O_{12}$ Solid Electrolytes and $LiCoO_2$ Cathodes for All-Solid-State Lithium-Ion Batteries, *J. Nanosci. Nanotechnol.*, 2020, **20**, 7002–7009.

103 Y. Liang, J. Cai, D. Liu and Z. Chen, Surface Modification of Nickel-Rich Cathode Materials by Ionically Conductive Materials at Room Temperature, *Energy Technol.*, 2021, **9**, 2100422.

104 P. Bunyanidhi, N. Phattharasupakun, C. Tomon, S. Duangdangchote, P. Kidkhunthod and M. Sawangphruk, Mechanofusing garnet solid electrolyte on the surface of Ni-rich layered oxide cathode towards high-rate capability of cylindrical Li-ion battery cells, *J. Power Sources*, 2022, **549**, 232043.

105 C. Shen, Y. Liu, W. Li, X. Liu, J. Xie, J. Jiang, Y. Jiang, B. Zhao and J. Zhang, One-pot synthesis and multifunctional surface modification of lithium-rich manganese-based cathode for enhanced structural stability and low-temperature performance, *J. Colloid Interface Sci.*, 2022, **615**, 1–9.

106 M. Yu, T. G. Brandt, E. Temeche and R. M. Laine, Stabilizing High-Voltage Cathodes via Ball-Mill Coating with Flame-Made Nanopowder Electrolytes, *ACS Appl. Mater. Interfaces*, 2022, **14**, 49617–49632.

107 W. Shu, Z. Jian, J. Zhou, Y. Zheng and W. Chen, Boosting the Electrochemical Performance of $Li_{1.2}Ni_{0.13}Co_{0.13}Mn_{0.54}O_2$ by Rough Coating with the Superionic Conductor $Li_7La_3Zr_2O_{12}$, *ACS Appl. Mater. Interfaces*, 2021, **13**, 54916–54923.

108 L. Huang, H. Fu, J. Duan, T. Wang, X. Zheng, Y. Huang, T. Zhao, Q. Yu, J. Wen, Y. Chen, D. Sun, W. Luo and Y. Huang, Negating Li^+ transfer barrier at solid-liquid electrolyte interface in hybrid batteries, *Chem*, 2022, **8**, 1928–1943.

109 E. J. Cheng, M. Shoji, T. Abe and K. Kanamura, Ionic liquid-containing cathodes empowering ceramic solid electrolytes, *iScience*, 2022, **25**, 103896.

110 Z. Lu, J. Yu, J. Wu, M. B. Effat, S. C. T. Kwok, Y. Lyu, M. M. F. Yuen and F. Ciucci, Enabling room-temperature solid-state lithium-metal batteries with fluoroethylene carbonate-modified plastic crystal interlayers, *Energy Storage Mater.*, 2019, **18**, 311–319.

111 K. Yoshima, Y. Harada and N. Takami, Thin hybrid electrolyte based on garnet-type lithium-ion conductor $Li_7La_3Zr_2O_{12}$ for 12 V-class bipolar batteries, *J. Power Sources*, 2016, **302**, 283–290.

112 H. Shin, S. J. Choi, S. Choi, B. Y. Jang, J. Jeong, Y.-G. Cho, S.-Y. Lee, H.-K. Song, J. H. Yu and T.-H. Kim, In situ gel electrolyte network guaranteeing ionic communication between solid electrolyte and cathode, *J. Power Sources*, 2022, **546**, 231926.

113 Z. Lin, X. Guo, R. Zhang, M. Tang, P. Ding, Z. Zhang, L. Wu, Y. Wang, S. Zhao, Q. Zhang and H. Yu, Molecular structure adjustment enhanced anti-oxidation ability of polymer electrolyte for solid-state lithium metal battery, *Nano Energy*, 2022, **98**, 107330.

114 Z. Li, Y. Lu, Q. Su, M. Wu, X. Que and H. Liu, High-Power Bipolar Solid-State Batteries Enabled by In-Situ-Formed Ionogels for Vehicle Applications, *ACS Appl. Mater. Interfaces*, 2022, **14**, 5402–5413.

115 M. Liu, W. Xie, B. Li, Y. Wang, G. Li, S. Zhang, Y. Wen, J. Qiu, J. Chen and P. Zhao, Garnet $Li_7La_3Zr_2O_{12}$-Based Solid-State Lithium Batteries Achieved by In Situ Thermally Polymerized Gel Polymer Electrolyte, *ACS Appl. Mater. Interfaces*, 2022, **14**, 43116–43126.

116 S. A. Pervez, B. P. Vinayan, M. A. Cambaz, G. Melinte, T. Diemant, T. Braun, G. Karkera, R. J. Behm and M. Fichtner, Electrochemical and compositional characterization of solid interphase layers in an interface-modified solid-state Li-sulfur battery, *J. Mater. Chem. A*, 2020, **8**, 16451–16462.

117 C. Shi, S. Takeuchi, G. V. Alexander, T. Hamann, J. O'Neill, J. A. Dura and E. D. Wachsman, High Sulfur Loading and Capacity Retention in Bilayer Garnet Sulfurized-Polyacrylonitrile/Lithium-Metal Batteries with Gel Polymer Electrolytes, *Adv. Energy Mater.*, 2023, **13**, 2301656.

118 L. Zhao, Y. Zeng, L. Fu, J. Zhang, D. Sun, Y. Tang, Y. Ren, F. Pan and H. Wang, Constructing Low-Impedance $Li_7La_3Zr_2O_{12}$-Based Composite Cathode Interface for All-Solid-State Lithium Batteries, *Small Struct.*, 2022, **3**, 2200200.

119 J. M. Zheng, X. B. Wu and Y. Yang, A comparison of preparation method on the electrochemical performance of cathode material $Li[Li_{0.2}Mn_{0.54}Ni_{0.13}Co_{0.13}]O_2$ for lithium ion battery, *Electrochim. Acta*, 2011, **56**, 3071–3078.

120 N. C. Rosero-Navarro, T. Yamashita, A. Miura, M. Higuchi, K. Tadanaga and J. W. Stevenson, Effect of Sintering Additives on Relative Density and Li-ion Conductivity of Nb-Doped $Li_7La_3Zr_2O_{12}$Solid Electrolyte, *J. Am. Ceram. Soc.*, 2017, **100**, 276–285.

121 M. B. Dixit, A. Parejiya, N. Muralidharan, R. Essehli, R. Amin and I. Belharouak, Understanding implications of cathode architecture on energy density of solid-state batteries, *Energy Storage Mater.*, 2021, **40**, 239–249.

122 H. Wakayama and Y. Kawai, The effect of the $LiCoO_2$/$Li_7La_3Zr_2O_{12}$ ratio on the structure and electrochemical properties of nanocomposite cathodes for all-solid-state lithium batteries, *J. Mater. Chem. A*, 2017, **5**, 18816–18822.

123 S. Pazhaniswamy, S. A. Joshi, H. Hou, A. K. Parameswaran and S. Agarwal, Hybrid Polymer Electrolyte Encased Cathode Particles Interface-Based Core-Shell Structure for High-Performance Room Temperature All-Solid-State Batteries, *Adv. Energy Mater.*, 2022, **13**, 2202981.

124 K. J. Kim and J. L. M. Rupp, All ceramic cathode composite design and manufacturing towards low interfacial resistance for garnet-based solid-state lithium batteries, *Energy Environ. Sci.*, 2020, **13**, 4930–4945.

125 F. Shen, R. A. Jonson, D. Y. Parkinson and M. C. Tucker, Preparing Li-garnet electrodes with engineered structures by phase inversion and high shear compaction processes, *J. Am. Ceram. Soc.*, 2021, **105**, 90–98.

126 M. Rosen, M. Finsterbusch, O. Guillon and D. Fattakhova-Rohlfing, Free standing dual phase cathode tapes-scalable fabrication and microstructure optimization of garnet-based ceramic cathodes, *J. Mater. Chem. A*, 2022, **10**, 2320–2326.

127 L. J. Miara, W. D. Richards, Y. E. Wang and G. Ceder, First-Principles Studies on Cation Dopants and Electrolyte|-Cathode Interphases for Lithium Garnets, *Chem. Mat.*, 2015, **27**, 4040–4047.

128 S. Smetaczek, E. Pycha, J. Ring, M. Siebenhofer, S. Ganschow, S. Berendts, A. Nenning, M. Kubicek, D. Rettenwander, A. Limbeck and J. Fleig, Investigating the electrochemical stability of $Li_7La_3Zr_2O_{12}$ solid electrolytes using field stress experiments, *J. Mater. Chem. A*, 2021, **9**, 15226–15237.

129 C. Wang, L. Zhang, H. Xie, G. Pastel, J. Dai, Y. Gong, B. Liu, E. D. Wachsman and L. Hu, Mixed ionic-electronic conductor enabled effective cathode-electrolyte interface in all solid state batteries, *Nano Energy*, 2018, **50**, 393–400.

130 F. Liang, Y. Sun, Y. Yuan, J. Huang, M. Hou and J. Lu, Designing inorganic electrolytes for solid-state Li-ion batteries: A perspective of LGPS and garnet, *Mater. Today*, 2021, **50**, 418–441.

131 J. Xiao, J. Han, C. Zhang, G. Ling, F. Kang and Q. H. Yang, Dimensionality, Function and Performance of Carbon Materials in Energy Storage Devices, *Adv. Energy Mater.*, 2021, **12**, 2100775.

132 R. Jalem, Y. Morishita, T. Okajima, H. Takeda, Y. Kondo, M. Nakayama and T. Kasuga, Experimental and first-principles DFT study on the electrochemical reactivity of garnet-type solid electrolytes with carbon, *J. Mater. Chem. A*, 2016, **4**, 14371–14379.

133 F.-M. Du, N. Zhao, R. Fang, Z.-H. Cui, Y.-Q. Li and X.-X. Guo, Influence of Electronic Conducting Additives on Cycle Performance of Garnet-based Solid Lithium Batteries, *J. Inorg. Mater.*, 2018, **33**, 462.

134 H.-M. Ryu, M. Y. Kim, H. Y. Jung, J. S. Lim, Y.-A. Kim and H.-S. Kim, Fabrication and electrochemical behavior of thin composite solid electrolyte for all-solid lithium batteries, *Ionics*, 2020, **26**, 2863–2874.

135 Y. N. Yang, Y. X. Li, Y. Q. Li and T. Zhang, On-surface lithium donor reaction enables decarbonated lithium garnets and compatible interfaces within cathodes, *Nat. Commun.*, 2020, **11**, 5519.

136 T. Liu, Y. Zhang, X. Zhang, L. Wang, S.-X. Zhao, Y.-H. Lin, Y. Shen, J. Luo, L. Li and C.-W. Nan, Enhanced electrochemical performance of bulk type oxide ceramic lithium batteries enabled by interface modification, *J. Mater. Chem. A*, 2018, **6**, 4649–4657.

137 George V. Alexander, N. C. Rosero-Navarro, A. Miura, K. Tadanaga and R. Murugan, Electrochemical performance of a garnet solid electrolyte based lithium metal battery with interface modification, *J. Mater. Chem. A*, 2018, **6**, 21018–21028.

138 Y. Xiao, L. J. Miara, Y. Wang and G. Ceder, Computational Screening of Cathode Coatings for Solid-State Batteries, *Joule*, 2019, **3**, 1252–1275.

139 J. Sastre, X. Chen, A. Aribia, A. N. Tiwari and Y. E. Romanyuk, Fast Charge Transfer across the $Li_7La_3Zr_2O_{12}$ Solid Electrolyte/$LiCoO_2$ Cathode Interface Enabled by an Interphase-Engineered All-Thin-Film Architecture, *ACS Appl. Mater. Interfaces*, 2020, **12**, 36196–36207.

140 Y. Ren and E. D. Wachsman, All Solid-State Li/LLZO/LCO Battery Enabled by Alumina Interfacial Coating, *J. Electrochem. Soc.*, 2022, **169**, 040529.

141 X.-L. Huang, X. Zhao, Z.-L. Wang, L.-M. Wang and X.-B. Zhang, Facile and controllable one-pot synthesis of an ordered nanostructure of $Co(OH)_2$ nanosheets and their modification by oxidation for high-performance lithium-ion batteries, *J. Mater. Chem.*, 2012, **22**, 3764–3769.

142 A. M. Nolan, E. D. Wachsman and Y. Mo, Computation-guided discovery of coating materials to stabilize the interface between lithium garnet solid electrolyte and

high-energy cathodes for all-solid-state lithium batteries, *Energy Storage Mater.*, 2021, **41**, 571–580.

143 E. Trevisanello, T. Ates, S. Passerini, F. H. Richter and J. Janek, Influence of the Polymer Structure and its Crystallization on the Interface Resistance in Polymer-LATP and Polymer-LLZO Hybrid Electrolytes, *J. Electrochem. Soc.*, 2022, **169**, 110547.

144 S. Mu, Z. Bi, S. Gao and X. Guo, Combination of Organic and Inorganic Electrolytes for Composite Membranes Toward Applicable Solid Lithium Batteries, *Chem. Res. Chin. Univ.*, 2021, **37**, 246–253.

145 L. Liu, D. Zhang, X. Xu, Z. Liu and J. Liu, Challenges and Development of Composite Solid Electrolytes for All-solid-state Lithium Batteries, *Chem. Res. Chin. Univ.*, 2021, **37**, 210–231.

146 A. R. Symington, M. Molinari, J. A. Dawson, J. M. Statham, J. Purton, P. Canepa and S. C. Parker, Elucidating the nature of grain boundary resistance in lithium lanthanum titanate, *J. Mater. Chem. A*, 2021, **9**, 6487–6498.

147 F. M. Pesci, A. Bertei, R. H. Brugge, S. P. Emge, A. K. O. Hekselman, L. E. Marbella, C. P. Grey and A. Aguadero, Establishing Ultralow Activation Energies for Lithium Transport in Garnet Electrolytes, *ACS Appl. Mater. Interfaces*, 2020, **12**, 32806–32816.

148 L. Cheng, W. Chen, M. Kunz, K. Persson, N. Tamura, G. Chen and M. Doeff, Effect of surface microstructure on electrochemical performance of garnet solid electrolytes, *ACS Appl. Mater. Interfaces*, 2015, **7**, 2073–2081.

149 C. Wang, W. Ping, Q. Bai, H. Cui, R. Hensleigh, R. Wang, A. H. Brozena, Z. Xu, J. Dai, Y. Pei, C. Zheng, G. Pastel, J. Gao, X. Wang, H. Wang, J.-C. Zhao, B. Yang, X. R. Zheng, J. Luo, Y. Mo, B. Dunn and L. Hu, A general method to synthesize and sinter bulk ceramics in seconds, *Science*, 2020, **368**, 521–526.

150 E. Ramos, A. Browar, J. Roehling and J. Ye, CO_2 Laser Sintering of Garnet-Type Solid-State Electrolytes, *ACS Energy Lett.*, 2022, **7**, 3392–3400.

151 M. Hong, Q. Dong, H. Xie, X. Wang, A. H. Brozena, J. Gao, C. Wang, C. Chen, J. Rao, J. Luo and L. Hu, Tailoring grain growth and densification toward a high-performance solid-state electrolyte membrane, *Mater. Today*, 2021, **42**, 41–48.

152 C. Zheng, Y. Lu, J. Su, Z. Song, T. Xiu, J. Jin, M. E. Badding and Z. Wen, Grain Boundary Engineering Enabled High-Performance Garnet-Type Electrolyte for Lithium Dendrite Free Lithium Metal Batteries, *Small Methods*, 2022, **6**, 2200667.

153 Z. Qin, X. Meng, Y. Xie, D. Qian, H. Deng, D. Mao, L. Wan and Y. Huang, Fast Li-ion transport pathways via 3D continuous networks in homogeneous garnet-type electrolyte for solid-state lithium batteries, *Energy Storage Mater.*, 2021, **43**, 190–201.

154 C. Zheng, J. Su, Z. Song, T. Xiu, J. Jin, M. E. Badding and Z. Wen, Improvement of density and electrochemical performance of garnet-type $Li_7La_3Zr_2O_{12}$ for solid-state lithium metal batteries enabled by W and Ta co-doping strategy, *Mater. Today, Energy*, 2022, **27**, 101034.

155 Y. Zhu, S. Wu, Y. Pan, X. Zhang, Z. Yan and Y. Xiang, Reduced Energy Barrier for Li^+ Transport Across Grain Boundaries with Amorphous Domains in LLZO Thin Films, *Nanoscale Res. Lett.*, 2020, **15**, 153.

156 M. Balaish, J. C. Gonzalez-Rosillo, K. J. Kim, Y. Zhu, Z. D. Hood and J. L. M. Rupp, Processing thin but robust electrolytes for solid-state batteries, *Nat. Energy*, 2021, **6**, 227–239.

157 L. H. Abrha, T. T. Hagos, Y. Nikodimos, H. K. Bezabh, G. B. Berhe, T. M. Hagos, C. J. Huang, W. A. Tegegne, S. K. Jiang, H. H. Weldeyohannes, S. H. Wu, W. N. Su and B. J. Hwang, Dual-Doped Cubic Garnet Solid Electrolytes with Superior Air Stability, *ACS Appl. Mater. Interfaces*, 2020, **12**, 25709–25717.

158 Y. Li, B. Xu, H. Xu, H. Duan, X. Lu, S. Xin, W. Zhou, L. Xue, G. Fu, A. Manthiram and J. B. Goodenough, Hybrid Polymer/Garnet Electrolyte with a Small Interfacial Resistance for Lithium-Ion Batteries, *Angew. Chem., Int. Ed.*, 2017, **56**, 753–756.

159 B. Xu, W. Li, H. Duan, H. Wang, Y. Guo, H. Li and H. Liu, Li_3PO_4-added garnet-type $Li_{6.5}La_3Zr_{1.5}Ta_{0.5}O_{12}$ for Li-dendrite suppression, *J. Power Sources*, 2017, **354**, 68–73.

160 Y. Ma, R. Bi, M. Yang, P. Wei, J. Qi, J. Wang, R. Yu and D. Wang, Hollow multishelled structural ZnO fillers enhance the ionic conductivity of polymer electrolyte for lithium batteries, *J. Nanopart. Res.*, 2023, **25**, 14.

161 J. Zheng and Y. Y. Hu, New Insights into the Compositional Dependence of Li-Ion Transport in Polymer-Ceramic Composite Electrolytes, *ACS Appl. Mater. Interfaces*, 2018, **10**, 4113–4120.

162 W. Hou, Y. Ou and K. Liu, Progress on High Voltage PEO-based Polymer Solid Electrolytes in Lithium Batteries, *Chem. Res. Chin. Univ.*, 2022, **38**, 735–743.

163 M. M. U. Din, M. Häusler, S. M. Fischer, K. Ratzenböck, F. F. Chamasemani, I. Hanghofer, V. Henninge, R. Brunner, C. Slugovc and D. Rettenwander, Role of Filler Content and Morphology in LLZO/PEO Membranes, *Front. Energy Res.*, 2021, **9**, 711610.

164 H. Huo, Y. Chen, J. Luo, X. Yang, X. Guo and X. Sun, Rational Design of Hierarchical ''Ceramic-in-Polymer'' and ''Polymer-in-Ceramic'' Electrolytes for Dendrite-Free Solid-State Batteries, *Adv. Energy Mater.*, 2019, **9**, 1804004.

165 J. Zagórski, B. Silván, D. Saurel, F. Aguesse and A. Llordés, Importance of Composite Electrolyte Processing to Improve the Kinetics and Energy Density of Li Metal Solid-State Batteries, *ACS Appl. Energy Mater.*, 2020, **3**, 8344–8355.

166 M. Wu, D. Liu, D. Qu, Z. Xie, J. Li, J. Lei and H. Tang, 3D Coral-like LLZO/PVDF Composite Electrolytes with Enhanced Ionic Conductivity and Mechanical Flexibility for Solid-State Lithium Batteries, *ACS Appl. Mater. Interfaces*, 2020, **12**, 52652–52659.

167 J. Cheng, G. Hou, Q. Chen, D. Li, K. Li, Q. Yuan, J. Wang and L. Ci, Sheet-like garnet structure design for upgrading PEO-based electrolyte, *Chem. Eng. J.*, 2022, **429**, 132343.

168 Z. Zhang, Y. Huang, G. Zhang and L. Chao, Three-dimensional fiber network reinforced polymer electrolyte for dendrite-free all-solid-state lithium metal batteries, *Energy Storage Mater.*, 2021, **41**, 631–641.

169 M. Zhang, P. Pan, Z. Cheng, J. Mao, L. Jiang, C. Ni, S. Park, K. Deng, Y. Hu and K. K. Fu, Flexible, Mechanically Robust, Solid-State Electrolyte Membrane with Conducting Oxide-Enhanced 3D Nanofiber Networks for Lithium Batteries, *Nano Lett.*, 2021, **21**, 7070–7078.

170 Z. Ren, J. Li, Y. Gong, C. Shi, J. Liang, Y. Li, C. He, Q. Zhang and X. Ren, Insight into the integration way of ceramic solid-state electrolyte fillers in the composite electrolyte for high performance solid-state lithium metal battery, *Energy Storage Mater.*, 2022, **51**, 130–138.

171 J. Hu, P. He, B. Zhang, B. Wang and L.-Z. Fan, Porous film host-derived 3D composite polymer electrolyte for high-voltage solid state lithium batteries, *Energy Storage Mater.*, 2020, **26**, 283–289.

172 T. Liu, Z. Chang, Y. Yin, K. Chen, Y. Zhang and X. Zhang, The PVDF-HFP gel polymer electrolyte for Li-O_2 battery, *Solid State Ion.*, 2018, **318**, 88–94.

173 H. Xie, Y. Bao, J. Cheng, C. Wang, E. M. Hitz, C. Yang, Z. Liang, Y. Zhou, S. He, T. Li and L. Hu, Flexible Garnet Solid-State Electrolyte Membranes Enabled by Tile-and-Grout Design, *ACS Energy Lett.*, 2019, **4**, 2668–2674.

174 P. Pan, M. Zhang, Z. Cheng, L. Jiang, J. Mao, C. Ni, Q. Chen, Y. Zeng, Y. Hu and K. Fu, Garnet ceramic fabric-reinforced flexible composite solid electrolyte derived from silk template for safe and long-term stable All-Solid-State lithium metal batteries, *Energy Storage Mater.*, 2022, **47**, 279–287.

175 J. Li, Y. Cai, Y. Cui, H. Wu, H. Da, Y. Yang, H. Zhang and S. Zhang, Fabrication of asymmetric bilayer solid-state electrolyte with boosted ion transport enabled by charge-rich space charge layer for -20 B 70 1C lithium metal battery, *Nano Energy*, 2022, **95**, 107027.

176 K. Nie, S. Wu, J. Wang, X. Sun, Z. Yan, J. Qiu, Q. Yang, R. Xiao, X. Yu, H. Li, L. Chen and X. Huang, Reaction Mechanisms of Ta-Substituted Cubic $Li_7La_3Zr_2O_{12}$ with Solvents During Storage, *ACS Appl. Mater. Interfaces*, 2021, **13**, 38384–38393.

177 L. Meabe, J. Zagorski, D. Mecerreyes and F. Aguesse, and L. L. A, New Insights on the Origin of Chemical Instabilities Between Poly(carbonate)-based Polymer and Li-containing Inorganic Materials, *ChemPhysChem*, 2022, **23**, e202200296.

178 Y. Gao, Z. Sun, C. Cui, H. Wang, W. Cao, Z. Hou, D. Zhu, Y. Yang and T. Zhang, An Ultrathin, Flexible Solid Electrolyte with High Ionic Conductivity Enhanced by a Mutual Promotion Mechanism, *ACS Appl. Mater. Interfaces*, 2022, **14**, 45373–45381.

179 D. Brogioli, F. Langer, R. Kun and F. La Mantia, Space-Charge Effects at the $Li_7La_3Zr_2O_{12}$/Poly(ethylene oxide) Interface, *ACS Appl. Mater. Interfaces*, 2019, **11**, 11999–12007.

180 W. P. Chen, H. Duan, J. L. Shi, Y. Qian, J. Wan, X. D. Zhang, H. Sheng, B. Guan, R. Wen, Y. X. Yin, S. Xin, Y. G. Guo and L. J. Wan, Bridging Interparticle Li^+ Conduction in a Soft Ceramic Oxide Electrolyte, *J. Am. Chem. Soc.*, 2021, **143**, 5717–5726.

181 Y. Xu, K. Wang, Y. An, W. Liu, C. Li, S. Zheng, X. Zhang, L. Wang, X. Sun and Y. Ma, Rapid Ion Transport Induced by the Enhanced Interaction in Composite Polymer Electrolyte for All-Solid-State Lithium-Metal Batteries, *J. Phys. Chem. Lett.*, 2021, **12**, 10603–10609.

182 H. Wang, H. Gao, X. Chen, J. Zhu, W. Li, Z. Gong, Y. Li, M. S. Wang and Y. Yang, Linking the Defects to the Formation and Growth of Li Dendrite in All-Solid-State Batteries, *Adv. Energy Mater.*, 2021, **11**, 2102148.

183 A. Badran, T. Clemenceau, N. Andriamady, D. Marshall and R. Raj, Current constriction of Li-ion transport across lithium metal-ceramic electrolyte interface: Imaged with X-ray Tomography, *MRS Commun.*, 2021, **11**, 283–287.

184 F. Han, A. S. Westover, J. Yue, X. Fan, F. Wang, M. Chi, D. N. Leonard, N. J. Dudney, H. Wang and C. Wang, High electronic conductivity as the origin of lithium dendrite formation within solid electrolytes, *Nat. Energy*, 2019, **4**, 187–196.

185 S. Kim, C. Jung, H. Kim, K. E. Thomas-Alyea, G. Yoon, B. Kim, M. E. Badding, Z. Song, J. Chang, J. Kim, D. Im and K. Kang, The Role of Interlayer Chemistry in Li-Metal Growth through a Garnet-Type Solid Electrolyte, *Adv. Energy Mater.*, 2020, **10**, 1903993.

186 D. Zhou, M. Zhang, F. Sun, T. Arlt, J. E. Frerichs, K. Dong, J. Wang, A. Hilger, F. Wilde, M. Kolek, M. R. Hansen, P. Bieker, I. Manke, M. C. Stan and M. Winter, Performance and behavior of LLZO-based composite polymer electrolyte for lithium metal electrode with high capacity utilization, *Nano Energy*, 2020, **77**, 105196.

187 X. Liu, R. Garcia-Mendez, A. R. Lupini, Y. Cheng, Z. D. Hood, F. Han, A. Sharafi, J. C. Idrobo, N. J. Dudney, C. Wang, C. Ma, J. Sakamoto and M. Chi, Local electronic structure variation resulting in Li 'filament' formation within solid electrolytes, *Nat. Mater.*, 2021, **20**, 1485–1490.

188 P. M. Veelken, M. Wirtz, R. Schierholz, H. Tempel, H. Kungl, R. A. Eichel and F. Hausen, Investigating the Interface between Ceramic Particles and Polymer Matrix in Hybrid Electrolytes by Electrochemical Strain Microscopy, *Nanomaterials*, 2022, **12**, 654.

189 Y. Lu, C.-Z. Zhao, J.-Q. Huang and Q. Zhang, The timescale identification decoupling complicated kinetic processes in lithium batteries, *Joule*, 2022, **6**, 1172–1198.

190 P. Barai, T. Rojas, B. Narayanan, A. T. Ngo, L. A. Curtiss and V. Srinivasan, Investigation of Delamination-Induced Performance Decay at the Cathode/LLZO Interface, *Chem. Mat.*, 2021, **33**, 5527–5541.

191 T. W. Heo, A. Grieder, B. Wang, M. Wood, T. Hsu, S. A. Akhade, L. F. Wan, L.-Q. Chen, N. Adelstein and B. C. Wood, Microstructural impacts on ionic conductivity of oxide solid electrolytes from a combined atomistic-mesoscale approach, *NPJ Comput. Mater.*, 2021, **7**, 214.

192 M. R. Bonilla, F. A. Garcia Daza, P. Ranque, F. Aguesse, J. Carrasco and E. Akhmatskaya, Unveiling Interfacial Li-

Ion Dynamics in $Li_7La_3Zr_2O_{12}$/PEO(LiTFSI) Composite Polymer-Ceramic Solid Electrolytes for All-Solid-State Lithium Batteries, *ACS Appl. Mater. Interfaces*, 2021, **13**, 30653–30667.

193 H. Kim, C. Im, S. Ryu, Y. J. Gong, J. Cho, S. Pyo, H. Yun, J. Lee, J. Yoo and Y. S. Kim, Interface Modeling via Tailored Energy Band Alignment: Toward Electrochemically Stabilized All-Solid-State Li-Metal Batteries, *Adv. Funct. Mater.*, 2021, **32**, 2107555.

194 K. Kim, A. Dive, A. Grieder, N. Adelstein, S. Kang, L. F. Wan and B. C. Wood, Flexible machine-learning interatomic potential for simulating structural disordering behavior of $Li_7La_3Zr_2O_{12}$ solid electrolytes, *J. Chem. Phys.*, 2022, **156**, 221101.

195 N. Zhao, W. Khokhar, Z. Bi, C. Shi, X. Guo, L.-Z. Fan and C.-W. Nan, Solid Garnet Batteries, *Joule*, 2019, **3**, 1190–1199.

196 J. Wan, J. Xie, X. Kong, Z. Liu, K. Liu, F. Shi, A. Pei, H. Chen, W. Chen, J. Chen, X. Zhang, L. Zong, J. Wang, L. Q. Chen, J. Qin and Y. Cui, Ultrathin, flexible, solid polymer composite electrolyte enabled with aligned nanoporous host for lithium batteries, *Nat. Nanotechnol.*, 2019, **14**, 705–711.

197 X. Liu, D. Ren, H. Hsu, X. Feng, G.-L. Xu, M. Zhuang, H. Gao, L. Lu, X. Han, Z. Chu, J. Li, X. He, K. Amine and M. Ouyang, Thermal Runaway of Lithium-Ion Batteries without Internal Short Circuit, *Joule*, 2018, **2**, 2047–2064.

198 D. H. Doughty and E. P. Roth, A General Discussion of Li Ion Battery Safety, *Electrochem. Soc. Interface*, 2012, **21**, 37–44.

199 J. M. Doux, H. Nguyen, D. H. S. Tan, A. Banerjee, X. Wang, E. A. Wu, C. Jo, H. Yang and Y. S. Meng, Stack Pressure Considerations for Room-Temperature All-Solid-State Lithium Metal Batteries, *Adv. Energy Mater.*, 2019, **10**, 1903253.

200 J. H. Cho, X. Xiao, K. Guo, Y. Liu, H. Gao and B. W. Sheldon, Stress evolution in lithium metal electrodes, *Energy Storage Mater.*, 2020, **24**, 281–290.

201 W. S. LePage, Y. Chen, E. Kazyak, K.-H. Chen, A. J. Sanchez, A. Poli, E. M. Arruda, M. D. Thouless and N. P. Dasgupta, Lithium Mechanics: Roles of Strain Rate and Temperature and Implications for Lithium Metal Batteries, *J. Electrochem. Soc.*, 2019, **166**, A89–A97.

202 M. Yamamoto, M. Takahashi, Y. Terauchi, Y. Kobayashi, S. Ikeda and A. Sakuda, Fabrication of composite positive electrode sheet with high active material content and effect of fabrication pressure for all-solid-state battery, *J. Ceram. Soc. Jpn.*, 2017, **125**, 391–395.

203 X. Hu, J. Yu, Y. Wang, W. Guo, X. Zhang, M. Armand, F. Kang, G. Wang, D. Zhou and B. Li, A Lithium Intrusion-Blocking Interfacial Shield for Wide-Pressure-Range Solid-State Lithium Metal Batteries, *Adv. Mater.*, 2023, 2308275.

204 M. Wang and J. Sakamoto, Correlating the interface resistance and surface adhesion of the Li metal-solid electrolyte interface, *J. Power Sources*, 2018, **377**, 7–11.

205 A. Sharafi and A. R. Drews, *US Pat.*, US2023063636, 2023.

206 H. Xu, Q. Zhu, Y. Zhao, Z. Du, B. Li and S. Yang, Phase-Changeable Dynamic Conformal Electrode/electrolyte Interlayer enabling Pressure-Independent Solid-State Lithium Metal Batteries, *Adv. Mater.*, 2023, **35**, 2212111.

207 T. Fuchs, C. G. Haslam, A. C. Moy, C. Lerch, T. Krauskopf, J. Sakamoto, F. H. Richter and J. Janek, Increasing the Pressure-Free Stripping Capacity of the Lithium Metal Anode in Solid-State-sssBatteries by Carbon Nanotubes, *Adv. Energy Mater.*, 2022, **12**, 2201125.

